Methane distribution and hydrochemistry in lake and sea ice from a region of thawing permafrost, Siberia

Master Thesis in Geoecology

Ines Nicole Spangenberg

Supervisors

Prof. Dr. Guido Grosse

Dr. Ellen Damm

University of Potsdam

Institute of Earth and Environmental Science

In cooperation with the

Alfred Wegener Institute Helmholtz Centre for Polar and Marine Research

Potsdam, October 2018

Abstract

Permafrost regions, and especially thermokarst lakes, play a major role in the global carbon cycle and in the context of global warming. Thermokarst lakes and lagoons are sources of methane to the atmosphere. This process is restricted by an ice cover during the winter. However, the fate of methane below and in the ice of shallow thermokarst lakes, lagoons and coastal waters is poorly understood.

This study focuses on winter ice from two different water bodies in a region of thawing permafrost in northeast Siberia. One is a shallow thermokarst lagoon and the other a bay underlain by submarine permafrost. The two water bodies are semi-closed and open water systems, respectively, with different stages of permafrost degradation. Ice cores were used as records of the freezing process and methane pathways. Hydrochemical parameters, as stable water isotope composition, electrical conductivity, dissolved organic carbon and temperature as well as methane concentrations and stable carbon isotopic signature in the ice were analyzed.

Measured parameters differed between and within the two water bodies. The hydrochemical parameters indicated freezing in a semi-closed system for the thermokarst lagoon, where ice growth eventually cuts off exchange between the lagoon and the sea. In the bay, hydrochemistry indicated an open system. Ice on both water bodies was mostly methane-supersaturated with respect to the atmospheric equilibrium concentration. Methane concentration in the ice of the Lagoon varied greatly with highest concentrations at the ice-water interface. Stable isotope signatures indicated that methane above the ice-water interface was oxidized to concentrations close to or below the calculated atmospheric equilibrium concentration. In comparison to the Lagoon, the Bay ice had generally lower methane concentrations. Nevertheless, methane oxidation in ice is a potentially effective process in decreasing methane concentrations in shallow thermokarst lagoons during the winter.

As further warming of the Arctic shortens the duration of ice cover, methane pathways will probably shift. An understanding of the limits of methane oxidation in lake and sea ice is critical to understand their role in mitigating Arctic feedbacks to global warming.

Zusammenfassung

Permafrostgebiete und insbesondere Thermokarst Seen spielen eine wichtige Rolle bei der Betrachtung des globalen Kohlenstoffkreislaufs und im Zusammenhang mit der globalen Erwärmung. Thermokarst Seen und Lagunen sind Quellen für Methan in der Atmosphäre. Dieser Prozess ist im Winter durch Eisbedeckung eingeschränkt. Allerdings ist der Verbleib von Methan, welches sich über den Winter unter und im Eis flacher Thermokarst Seen, Lagunen und Küstengewässer akkumuliert, kaum erforscht. Diese Arbeit befasst sich mit der Wintereisbildung von zwei unterschiedlichen Gewässern, einer flachen Thermokarst Lagune und einer Bucht in einem submarinen Permafrostgebiet. Die Lagune stellt ein teilweise geschlossenes und die Bucht ein offenes System dar und die Gewässer zeigen unterschiedliche Stadien der Permafrostdegradierung. Um die Prozesse während der Eisbildung und Änderungen in der Methankonzentration nachzuverfolgen, wurden Eiskerne genutzt, die diese Prozesse über den Winter aufzeichnen. Hydrochemische Parameter, wie stabile Wasserisotope, elektrische Leitfähigkeit, gelöster organischer Kohlenstoff und Temperatur, als auch Methankonzentrationen und stabile Kohlenstoffisotopie des Methans wurden analysiert. Die gemessenen Parameter unterscheiden sich zwischen und innerhalb der Gewässer. Die hydrochemischen Parameter zeigen das Gefrieren in einem teilweise Geschlossenen System für die Thermokarst Lagune, wobei durch das Eiswachstum die Verbindung zwischen der Lagune und der Bucht geschlossen wird. Die Bucht ist hingegen ein offenes System, was auch die hydrochemischen Parameter wiederspiegeln. Das Eis der beiden Gewässer zeigt meist Methanübersättigung gegenüber der atmosphärischen Gleichgewichtskonzentration. Die Methankonzentrationen im Eis der Lagune zeigen große Schwankungen mit den höchsten Konzentrationen an der Eis-Wasser Grenzfläche. Die Signatur der stabilen Kohlenstoffisotope zeigt Methanoxidation oberhalb der Eis-Wasser Grenzfläche, teilweise bis hin zu Konzentrationen wie die berechnete atmosphärische Gleichgewichtskonzentration. Die Eiskerne der Bucht zeigen im Vergleich zur Lagune generell geringe Methankonzentrationen. Methanoxidation ist potenziell ein effektiver Prozess um Methankonzentrationen in Thermokarst Lagunen über den Winter zu verringern. Die zunehmende Erwärmung der Arktis verkürzt die Eisbedeckungszeit, wodurch eine Veränderung der Methanflüsse zu erwarten ist. Das Verständnis von Methanoxidation im Eis arktischer Gewässer ist wichtig um ihre Rolle der arktischen Rückkopplung auf die Klimaerwärmung zu verstehen.

Table of Contents

List of Figures

List of Tables

1 Introduction

1.1 Relevance of the topic

Methane (CH_4) is, after water vapor and carbon dioxide (CO_2), the most abundant greenhouse gas in the troposphere (Wuebbles & Hayhoe, 2002). When averaged over a 100 year timescale, the warming effect of CH_4 per unit mass is 28 times higher than that of CO_2 (IPCC, 2013). Permafrost regions are of particular concern when considering future climate, as large reservoirs of organic carbon resides therein. Especially the Yedoma (windblown dust deposition during the glacial age in Siberia and Central Alaska), is a large storage of carbon as it is rich in organic materials (Zimov et al., 2006). Therefore, those regions play an important role in the global carbon cycle and for the processes of global warming (Schuur et al., 2008).

The warming of the Arctic is causing permafrost throughout the Arctic to thaw, leading to the release of greenhouse gases such as CH_4 and CO_2 (Koven et al., 2011). As a result of warming temperatures the organic carbon stored in permafrost becomes available for microbial decomposition and the production of greenhouse gases (Schuur et al., 2015). This Arctic source in particular may contribute to Arctic amplification of global warming as significant greenhouse gas emissions into the atmosphere may generate positive feedbacks to global warming (ICCP, 2013).

Warming also leads to further formation of thermokarst lakes in ice-rich permafrost regions which are significant sources of CH_4 (Karlsson et al., 2013; Walter et al., 2007a). These lakes have particularly high emissions because they release CH_4 produced from organic matter previously sequestered in permafrost (Walter et al., 2007b).

The amount of CH_4 emitted from Arctic lakes to the atmosphere is uncertain but is expected to increase as a result of arctic warming (Bastviken et al., 2004; Boereboom et al., 2012; Cole et al., 2007; Walter et al., 2006). As there is strong evidence that seasonally ice-covered northern lakes are globally abundant, they are expected to play an important role in the global carbon cycle (Karlsson et al., 2013). Zimov et al. (1997) state that Siberian Lakes act as a large winter source for CH_4. Therefore greater understanding of annual CH_4 emission budgets from northern water bodies is necessary to better simulate future climate scenarios (Zhou et al., 2014).

Surprisingly, CH_4 concentrations at 65° to 70°N are highest from March to April (Fung et al., 1991). Studies in recent years have illustrated the importance of the winter period for annual CH_4 and CO_2 emission budgets of northern lakes, as they certainly produced CH_4 over winter, but the processes contributing to CH_4 and CO_2 dynamics in this period are barely understood

(Denfeld et al., 2018; Powers & Hampton, 2016). Since Arctic waters are covered with ice for 9-10 months, the ice-covered period dominates the year. This emphasize the relevance of winter studies for Artic regions.

1.2 Previous research and gaps

Previous work has focused on CH_4 bubbles in lake ice (Walter et al., 2006; Wik et al., 2011) and CH_4 accumulation under lake ice (Boereboom et al., 2012; Langer et al, 2015). Several studies suggested CH_4 ebullition from the sediments to the water-ice interface in lakes over winter, as the bubbles are trapped in the ice (Sasaki et al., 2009; Walter Anthony et al., 2010; Walter et al., 2008; Walter et al., 2006; Walter, et al., 2007; Wik et al., 2011). Remote sensing was effectively used for detecting CH_4 bubbles in thermokarst lake ice from Alaska (Lindgren et al., 2016). However, limited studies have focused on the fate of CH_4 accumulation under the ice over winter.

Some studies have used ice as a natural environmental record of CH_4 concentrations to draw inferences about winter processes and to compare water bodies. CH_4 distribution in ice cores and under ice were analysed in shallow ice-covered tundra lakes in Alaska (Phelps et al., 1998). Boereboom et al. (2012) examined CO_2 and CH_4 in the ice of four different lakes in a discontinuous permafrost area. In both studies the accumulation of CH_4 under the ice during winter was investigated.

Other studies show that a high CH_4 emission rate occurs during ice melt in spring of high latitude lakes (Karlsson et al., 2013; Michmerhuizenet al., 1996). However, CH_4 oxidation may limit the CH_4 amount emitted from the water to the atmosphere during ice melt (Ricão Canelhas et al., 2016). CH_4 oxidation processes are also observed in Arctic shelf waters (Damm et al., 2005; Mau et al., 2013), as well as in lakes (Bastviken et al., 2002; Lidstrom & Somers, 1984) and at the water-ice interface (Martinez-Cruz et al., 2015; Ricão Canelhas et al., 2016). While Phelps et al. (1998) suggest that methanotrophic activity is inhibited in cold waters, CH_4 is also oxidized at temperatures as low as 2°C (Ricão Canelhas et al., 2016). The internal CH_4 flux in water bodies is dominated by CH_4 production (methanogenesis) and CH_4 consumption (oxidation) (Denfeld et al., 2018). Shallow lakes, i.e. thermokarst lakes seem to be CH_4 sources throughout the whole year (Wik et al., 2016). CH_4 is assumed to be produced mainly in the anoxic sediments (e.g. Rudd & Hamilton, 1978). The pathways from the sediments to the water column are diffusion and ebullition (Bastviken et al., 2008). The production of CH_4 is temperature dependent (Kelly & Chynoweth, 1981; Zeikus & Winfrey, 1976), but CH_4 ebullition and accumulation under ice suggest CH_4 production continues during winter (Walter

Anthony et al., 2010). In shallow lakes, a large amount of CH_4 is bubbling from the sediments to the water column surface (Zimov et al., 2006). Gas may easily escape from the water to the atmosphere in summer, whereas an ice cover forms a barrier in winter. Thus, bubbles get trapped in or under the ice (Walter et al., 2008). This enhances CH_4 oxidation at the ice-water interface (Ricão Canelhas et al., 2016; Rudd & Hamilton, 1978), but the circumstances in which CH_4 oxidation occurs at the ice-water interface are poorly understood (Ricão Canelhas et al., 2016). Furthermore, differences between CH_4 accumulation in ice on different types of Arctic water bodies (e.g. ponds, lakes, lagoons, coastal waters) have not been studied yet. The fate of CH_4 for ice covered water bodies of coastal permafrost regions (i.e. shallow thermokarst lakes, lagoons and coastal waters) is highly unknown. As these regions are highly vulnerable to warming, it is important to fill this knowledge gap in order to predict CH_4 emissions in a warming climate.

Only few studies compare ice from different Arctic water bodies. As the internal CH_4 fluxes in lakes are coupled to their limnological and geomorphological characteristics (Bastviken et al., 2008; Bastviken et al., 2004; Boereboom et al., 2012; Denfeld et al., 2018), studies of different water bodies are needed and offer a means to compare and understand CH_4 fluxes in different limnological systems.

1.3 Objectives of this study

The aim of this study is to investigate the CH_4 distribution of floating ice from two different water bodies in a region of thawing permafrost in northeast Siberia and to discuss the influence of freezing processes and oxidation on CH_4 accumulation in the ice. The following research questions are discussed:

1) What influenced the freezing processes in the two water bodies?
2) Is the freezing process a crucial factor for the CH_4 concentration in the ice?
3) What role does CH_4 oxidation play in the two water bodies?
4) What are the causes of differences in CH_4 concentrations and stable carbon isotopic signature of CH_4 ($\delta^{13}C_{CH4}$) between water body types?

2 Study Area

The study area is the southern coast of the Bykovsky Peninsula between 71° 40’ - 71° 80’ N and 129° 00’ - 129° 30’ E, in northern Siberia. The two investigated coastal water bodies are Polar Fox Lagoon and Tiksi Bay (**Figure 1**). The Bykovsky Peninsula is located north-east of the harbor town of Tiksi (Lantuit et al., 2011) and approximately 20 km southeast of the Lena River Delta (Grosse et al., 2006).

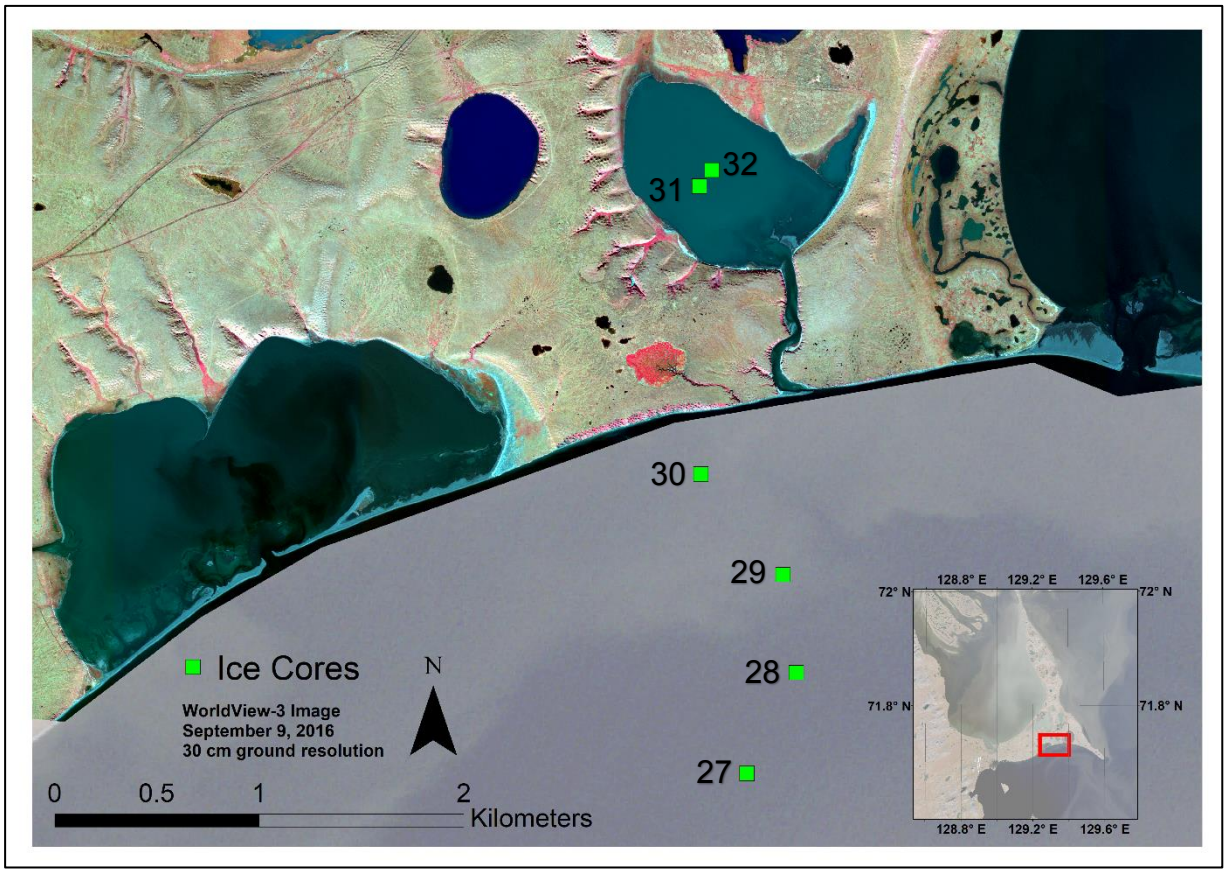

Figure 1: Map of the study area and ice core locations (green squares) for Polar Fox Lagoon (31, 32) and Tiksi Bay (27 - 30) (mapped by M. Angelopoulos).

Geology and geomorphology

The region’s surface deposits belong to a Pleistocene accumulation plain (Schirrmeister et al., 2010). This area is part of the recent coastal lowland of the Laptev Sea (Grosse et al., 2005) and characterized by continuous, ice-rich permafrost (Meyer et al., 2002). The continuous permafrost zone reaches depths of 500 - 600 m in the region. The thickness of the active layer reaches up to 50 cm (Grosse et al., 2005). The Bykovsky Peninsula is characterized by the Ice Complex, a stratigraphic unit formed by polygonal ice wedges with very ice-rich sediments (Schirrmeister et al., 2002). Therefore, this region is subject to thermo-erosion (erosion due to melting of ground ice) and thermokarst (land surface subsidence due to the melting of ground

ice) (Günther et al., 2013; Günther et al., 2015). The high ice content leads to thermo-abrasion of the coast (Günther et al., 2015; Lantuit et al., 2011). Today, the Ice Complex is preserved in elevated erosional remnants in thermokarst landscapes called Yedoma hills as well as on cryoplanation terraces (Schirrmeister et al., 2010). The land surface elevation of Bykovsky Peninsula is dominated by flat elevated areas up to 40 m a.s.l., as well as thermokarst depressions down to sea level (Grosse et al., 2006) (**Figure 2**). The material is organic-rich, as the deposits contain buried cryosols and peat horizons (Schirrmeister et al., 2010).

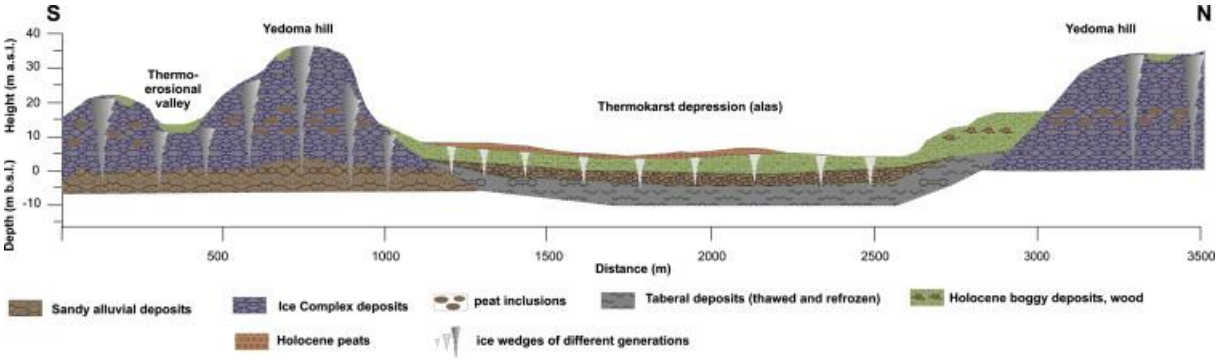

Figure 2: Schematic sketch of the Bykovsky Peninsula morphology (Schirrmeister et al., 2010).

Numerous thermokarst lakes have formed on the Bykovsky Peninsula due to the thawing of the Ice Complex. The transformation of thermokarst lacustrine depressions into thermokarst lagoons occurs when a connection between the lacustrine depression and the open sea is made, probably as a result of thermokarst processes (Romanovskii et al., 2000).

Polar Fox Lagoon is such a thermokarst lagoon, and it is evident from its morphology that it formed in a thermokarst depression (alas). At the exposed shoreline, it is evident that the lower extent of the ice-rich sediments and the thermokarst lake beds lie below sea level. This matches observations along the Bykovsky Peninsula coastline, where the Ice Complex also extends downward below modern sea level (Günther et al., 2015). Polar Fox Lagoon remains connected to Tiksi Bay by a shallow (< 50 cm deep) channel. Thermokarst lacustrine depressions that are transformed into thermokarst lagoons may be subsequently affected by seawater, at least intermittently, during high water events such as storm surges, resulting in changes to their temperature and salinity regimes (Romanovskii et al., 2000).

Tiksi Bay is a relatively shallow bay in the south of the peninsula, at the east partially underlain by submarine permafrost (Overduin et al., 2012). The bay is located south of the Bykovskaya Channel, the major discharge mouth of the Lena River, and is therefore influenced by the spring discharge of the Lena River. About 25 % of the Lena's spring discharge exits the delta through the south-eastern Bykovskaya Channel (Fedorova et al., 2015). This causes the presence of brackish water in the bay (Lantuit et al., 2011) with measured electrical conductivity over

10.0 mS cm^{-1} for the eight months of low-temperature water at the outlet of the Bykovskaya Channel. Tiksi Bay belongs to the Buor Khaya Bay region, where the water column is usually stratified, with a colder, more saline water underlying the brackish surface layer (Overduin et al., 2015b). The depth of the pycnocline varies between 4 and 10 m and the stratification can be disturbed by storm events. The sea level at Tiksi Bay is also influenced by storm events. On average, maximum wave heights are about 1.1 m during storms in the Tiksi Bay. Tidally-based sea-level oscillations have little influence on the height of storm surges, as the tidal regime in the Bykovsky Peninsula region is micro-tidal (Lantuit et al., 2011).

Climatology

In the region, large seasonal temperature variations occur, with mean annual temperatures of –12 °C (Lantuit et al., 2011). It is a highly continental climate with January as the coldest month (mean temperature –31.1 °C) and July as the warmest month (mean temperature 7.8 °C) (Meyer et al., 2002). In the southern Laptev Sea, the sea ice season extends on average from middle October to middle June (Lantuit et al., 2011).

3 Methods

3.1 Sampling in the field

The ice cores were taken with a Kovacs Mark II ice coring system (9 cm diameter), between the 5th of April and the 12th of April 2017. Cores were collected in triplicate from each sampling site. One core was used for temperature measurements, one was collected for genetic studies, and the third was used in this study. Immediately after sampling, temperature was measured by drilling holes into one of the cores and inserting a digital thermometer. Cores were wrapped in sealed plastic tubes and packed in thermally insulated boxes for the transport to Germany. When they arrived in Germany, most cores were missing three sections, which had previously been sampled in the field at the Research Station Samoylov Island in the Lena Delta (Boike et al., (eds), in prep.). 10 cm had been removed from the top and middle and the lowermost 30 cm of the cores were removed. Further information about the field work and the sampling can be found in the Bykovsky 2017 spring expedition report (Boike et al., (eds), in prep.).

3.2 Sample processing

The ice cores were processed in Potsdam from the 4th until the 15th of December 2017. In a –15°C cold room of the Geoforschungszentrum Potsdam the ice cores were cut with a band saw approximately every 10 cm and stored for melting in gas-tight TEDLAR bags. The closed bags were evacuated with a vacuum pump. The samples were left outside at 4 - 7 °C to melt overnight and during the next day. Due to warmer outdoor temperatures, the second set of cores was melted in a 4 °C cold room. After melting, the bags were shaken and water was filled gently, without producing bubbles, into 100 mL glass bottles for the analysis of CH_4 concentrations and $\delta^{13}C$ in CH_4. The remaining water was distributed into other sample bottles for hydrochemical measurements of pH, electrical conductivity (EC), dissolved organic carbon (DOC), $\delta^{18}O$ and δD isotopes of water, as well as major anion and cation concentrations.

3.3 Hydrochemistry in ice

The hydrochemical parameters were measured at the laboratory for hydrochemistry at the Alfred Wegener Institute in Potsdam.

EC and pH were measured with a WTW Multilab 540 measuring device as soon as possible after bottling. The salinity was calculated from the values of the electrical conductivity after MacDougall & Barker (2011). The samples for DOC were filtered with 0.7 µm pore size glass fiber filters (the filters were first rinsed with 20 mL of the sample), filled in 20 mL glass-headspace vials and closed with aluminum crimp caps. For preservation, 50 µl of 30 % HCl

supra-pure were added to the sample before closing the vials, which were stored at 4 °C until measuring. DOC was measured with a Shimadzu Total Organic Carbon Analyzer (TOC-VCPH). The average of three to five injections per sample was used as the measured value. The detection limit for the DOC measurement is 0.25 mg L^{-1} and the uncertainty of the measurement is ± 10 % of the measured value, for values higher than 1.5 mg L^{-1} and for values lower than 1.5 mg L^{-1} ± 15-20 %.

For cation and anion concentrations the samples were filtered with 0.45 µm pore size cellulose acetate filters (the filters were first rinsed with 5 - 10 mL sample). 15 mL of the sample was filled in centrifuge tubes and preserved with 100 µl of 65 % HNO_3 supra-pure (cations), also stored at 4 °C until measuring, and 8 mL was filled in H/LDPE wide mouth bottles (anions) without any preservation and frozen until measuring. Anion concentrations were analyzed with ion chromatography (IC) using a DIONEX/Thermo ICS-2100 measuring device. For the analyses of the cation concentrations the samples were measured with inductively coupled plasma optical emission spectrometry (ICP-OES) on a Perkin Elmer Optima 8300DV.

Stable water isotopes ($\delta^{18}O$ and δD) were measured at the laboratory for stable water isotopes at the Alfred Wegener Institute in Potsdam. To measure stable water isotopes, 10 mL of the untreated water sample was filled in 10 mL PE narrow neck bottles. Samples with higher salinity were measured with an Isotope Ratio Mass Spectrometer (IRMS: Delta-S (DIFE)), whereas samples with low salinity were measured with an Ultra High-Precision Isotopic Water Analyzer (PICARRO L2130-*i*).

3.4 Dissolved methane concentration

Meltwater from the TEDLAR bags was filled until overflowing in 100 mL glass bottles, sealed with butyl stoppers and crimped with aluminum plugs. The samples were kept cold (4 °C) and dark until the measurements were done at the lab (max. 2 months between sampling and measurement). CH_4 concentrations were measured at the Alfred Wegener Institute in Bremerhaven during the periods 29th January to the 2nd of February 2018 and 19th to the 21st of February 2018. For the CH_4 concentration, 5 mL of N_2 was added into the vials, and then equilibrated for 1 hour at room temperature. Normally, 1.5 mL of a sample was injected into a gas chromatograph (GC; Agilent 8900) with a flame ionization detector (FID). For gas chromatographic separation, a packed column (Porapac Q 80/100 mesh) was used. The GC was operated isothermally (60°C) and the FID was held at 250 °C. Standards of 1.665, 4.99, 10, 24.97, 50.09 and 100 ppm gas mixture were used for calibration, with triplicate measurements

of each standard. **Figure 3** shows the calibration line for the 30th of January 2018. The standard deviations on this date were 0.017, 0.531, 0.026, 0.144, 0.052 and 0.309 ppm, respectively.

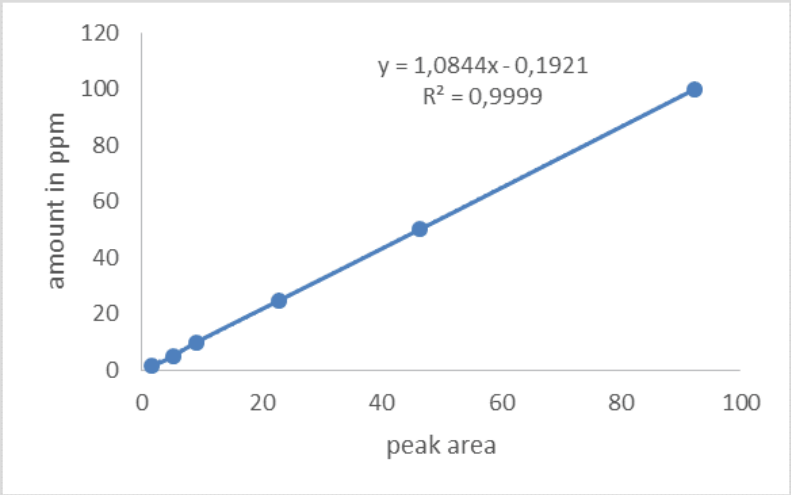

Figure 3: Calibration line for the GC of the 30th January 2018 with the peak area versus the concentration of methane in ppm.

We calibrated the GC on the 30th of January and the 19th of February. Between the measurements, we repeated the 1.665 ppm and 4.99 ppm standard three times to check the calibration. The GC precision had an error of 1 %. 40 % (n = 28) of the samples had CH_4 concentrations below the lowest standard of 1.665 ppm (ranging from 0.7 ppm to 1.6 ppm), while 3 % (n = 2) had concentrations exceeding the highest standard (ranging from 105 ppm to 2723 ppm).

3.5 Carbon isotopic signal of methane

The $\delta^{13}C_{CH4}$ values were measured on the same day as the CH_4 concentrations. After measuring the CH_4 concentration, 20 mL N_2 was added to the sample bottle to increase the headspace of the bottle for stable carbon isotope measurements. The bottle was shaken for at least 30 minutes. 20 mL gas was removed with a glass syringe by adding 20 mL of Milli-Q water at the same time to equilibrate pressure. The $\delta^{13}C_{CH4}$ values were determined using a Delta XP plus Finnigan mass spectrometer. The extracted gas was purged and trapped with PreCon equipment (Finnigan) to pre-concentrate the sample. All isotopic ratios are relative to the Vienna Pee Dee Belemnite (VPDB) standard using the conventional δ-notation. The analytical error of the analyses is ± 1.5 ‰ for $\delta^{13}C_{CH4}$ values.

Calculation of the methane concentration in nM

The calculation of the CH_4 concentration in nM is based on the method presented in Wiesenburg & Guinasso (1979). By known volumes of the gas and water phase in the bottle the CH_4 concentrations for both phases were calculated from the measured ppm values. The Bunsen solubility coefficient (*ln ß)*, was used to calculate the CH_4 concentration in the water (C_W) in liter, from measured CH_4 concentrations in the headspace of the sample bottles (C_m) in ppm, assuming water-air equilibrium between the water and headspace in the sample bottles. The Bunsen coefficient is given by

$$ln\,ß = A_1 + A_2(\frac{100}{T}) + A_3\,ln(\frac{T}{100}) + S[B_1 + B_2(\frac{T}{100}) + B_3(\frac{T}{100})^2] \quad (1)$$

where A_1, A_2, A_3, B_1, B_2, and B_3 are constants described in Wiesenburg & Guinasso (1979), T is the temperature in Kelvin during the measurement of the sample and S is the salinity in parts per thousand. To calculate the concentration of CH_4 in the water phase (C_W), the Bunsen solubility coefficient *ln ß* was multiplied by C_m in ppm $*10^{-6}$ and the volume of the water sample (V_W):

$$C_W = \ln \beta\, C_m V_W \times 10^{-6} \quad (2)$$

The CH_4 concentration in the gas phase (C_g) was calculated by C_m in ppm $*10^{-6}$ multiplied by the volume of the headspace (V_h) in liter:

$$C_g = C_m \times 10^{-6} \times V_h \quad (3)$$

The total CH_4 concentration in water and air from the sample bottle, n in mol, was computed by the use of the ideal gas law, with laboratory conditions of p *(101.325 Pa)* and T *(293.15 K)*, and calculated in nM (C_{tot}):

$$n = \frac{p(C_g + C_w)}{RT} \quad (4)$$

$$C_{tot} = (\frac{n}{V_w}) \times 10^9 \quad (5)$$

which is the concentration of CH_4 in the ice reported in this study.

3.6 Data treatment

The data are compared within ice cores as a function of depth below the ice surface and between the cores of one water body (Polar Fox Lagoon or Tiksi Bay). For a simple comparison between ice cores and the two water bodies, mean values and the range (min., max. values) were calculated for every core (**Table 2, Table 3**).

In addition, existing data on water temperature, EC, stable isotope composition and CH_4 concentrations available from the literature or reports of other expeditions to the region were used to discuss the data.

4 Results

4.1 Description of the ice cores

For the results of this study, six ice cores were recovered in total: two from Polar Fox Lagoon and four from Tiksi Bay. The cores from Polar Fox Lagoon were both from the middle of the lagoon. The cores from Tiksi Bay were taken in a transect with differing distances to the shore (27 - 30, **Figure 1)**. **Table 1** lists the length of the recovered samples for each core. Some sections were already cut in the field from the top, middle and bottom of each core (except for core 32) so that the top 10 cm, 10 cm in the middle and the lowermost 30 cm are missing from cores 27, 28, 29, 30 and 31. Only stable water isotope measurements and temperature data exist for all depths from all cores. As the cores were sampled in approximately 10 cm sections and samples were well-mixed, one data point in the figures represents a mean value for a section of 10 cm of one ice core. A table with all measured values is shown in the appendix (**Table 4**). The cores were divided into three portions with depth – upper, lower and bottom – as these represent different freezing times. The upper portion illustrates the oldest, first formed ice. The lower portion was formed afterwards. The bottom ice shows the youngest ice.

Table 1: Overview of the length and recovered sample sections for the analyzed ice cores.

Core	Total length (cm)	Samples recovered (cm)
27	155	10-20, 20-30, 30-40, 40-50, 50-60, 60-70, 80-90, 90-100, 100-110, 110-120
28	151	10-19, 19-30, 30-42, 42-51, 51-60, 60-69, 80-90, 90-100, 100-110, 110-121
29	135	10-20, 20-30, 30-42, 42-50, 50-58, 71-80, 80-95, 95-105
30	143	10-20, 20-30, 30-38, 42-50, 50-60, 60-70, 80-88, 88-95, 95-105, 105-115
31	167	10-20, 20-30, 30-40, 40-50, 50-60, 60-70, 70-80, 90-100, 100-110, 110-120, 120-130, 130-140
32	164	10-20, 20-30, 30-40, 40-52, 52-62, 62-72, 72-82, 82-93, 93-104, 104-114, 114-122, 122-131, 131-140, 140-148, 148-156, 156-164

4.2 Hydrochemistry in the ice of Polar Fox Lagoon

Stable water isotopes

The stable water isotopic signal of the two cores of the Polar Fox lagoon were in a comparable range (**Figure 4**, **Table 2**). The measured values of both cores were between –17.1 ‰ and –15.0 ‰ for $\delta^{18}O$ and –129.1 ‰ to –114.3 ‰ for δD (**Table 2**). The values of both, $\delta^{18}O$ and δD, showed a different trend between the upper (0 – 60 ± 2 cm) and the lower ice (> 60 ± 2 cm) (**Figure 4**, left and middle). In the upper portion of the ice, $\delta^{18}O$ values changed to slightly lighter values from –16.0 ‰ to –16.6 ‰ (core 32), but $\delta^{18}O$ values were almost stable with –16.5 ‰ and –16.6 ‰ (core 31) from 0 - 10 cm to 10 - 20 cm, whereas the δD values decreased slightly in both cores, with –124.5 ‰ to –127.4 ‰ (core 32) and –126.6 ‰ to –127.7 ‰ (core 31). Between 10 - 20 cm and 50 - 60 ± 2 cm the oxygen and hydrogen isotopes increased towards values of –15.2 ‰ ($\delta^{18}O$, core 31) and –15.0 ‰ ($\delta^{18}O$, core 32), as well as –116.2 ‰ (δD, core 31) and –114.3 ‰ (δD, core 32). In contrast, the stable water isotopic composition decreased in the lower portion, below the depth of 60 ± 2 cm towards the bottom of the ice cores. For both cores (core 31, 32), the lowest values occurred at the bottom, with about –17 ‰ ($\delta^{18}O$) and –129.5 ‰, (δD) for the depths 147 - 157 cm, 157 - 167 cm and 148-156 cm, 156 - 164 cm, respectively.

The deuterium excess (d-excess) is defined as d-excess = δD - 8 $\delta^{18}O$ (Dansgaard, 1964) and ranged from 3.9 ‰ to 8.7 ‰ (**Table 2**) for both cores. **Figure 4** (right) presents the distribution of the d-excess with depth. Between 0 - 10 cm and 10 - 20 cm, the d-excess was almost stable with values of 5.1 ‰ and 4.7 ‰ for core 31 and increased from 3.9 ‰ to 5.3 ‰ for core 32. With values about 5 ‰, the d-excess was almost stable between 0 - 90 cm (core 31) and 20 - 82 cm (core 32). Below the depth of 80 - 90 cm (core 31) and 72 - 82 cm (core 32), the d-excess increased with depth from 5.5 ‰ to 7.2 ‰ (core 31) and ~7.6 ‰ (core 32) in the lower portion of the ice, except for higher values of 7.3 ‰ and 7.6 ‰ at core 31 (110 - 120 cm, 120 - 130 cm) and 8.7 ‰ at core 32 (131 - 140 cm).

Electrical conductivity and salinity

The EC of Polar Fox Lagoon ranged from 101 µS cm^{-1} to 3630 µS cm^{-1} for both cores (**Table 2**). In both cores, EC varied similarly: a general trend of increase with depth (**Figure 5**, left). The EC was lower in the upper portion of the ice and highest at the bottom.

Core 31 had the lowest values for the EC with 101.2 µS cm^{-1} at the depths of 10 - 20 cm and ranged to 645 µS cm^{-1} in 20 - 30 cm. Values between 1056 µS cm^{-1} and 1836 µS cm^{-1} occurred at the depths between 20 - 30 cm and 70 - 80 cm. The EC was even higher with values from

2492 µS cm^{-1} to 3630 µS cm^{-1} between the depths of 80 - 90 cm and 130 - 140 cm. The highest value appeared with 3630 µS cm^{-1} at the depth of 120 - 130 cm but the EC of the last measured depth (130-140 cm) was almost the same with values of 3610 µS cm^{-1}. The EC of core 32 ranged from 101.5 µS cm^{-1} to 860 µS cm^{-1} between the depths from 0 - 40 cm, but with a higher value of 797 µS cm^{-1} at the depth of 0 - 10 cm than at the depths of 10 - 20 cm and 20 - 30 cm (101.5 µS cm^{-1} and 577 µS cm^{-1}). Between the depths of 40 - 104 cm, EC values were higher and ranged from 1144 µS cm^{-1} to 2252 µS cm^{-1}. Values above 2500 µS cm^{-1} occurred from 104 - 164 cm, with the highest value of 3520 µS cm^{-1} at the bottom of the core (156 - 164 cm).

The salinity was lower than 0.5 PSU at the depths from 10 - 40 cm (core 31) and 0 - 40 cm (core 32), whereas PSU values higher than 0.5 PSU were measured at the depths below 80 cm for both cores. At the depths between 80 - 140 cm (core 31) and 82 - 164 cm (core 32), values above 1 PSU occurred, whereas the salinity values of the depths of 120 - 130 cm, 130 - 140 cm (core 31) and 156 - 164 cm (core 32) were about 2 PSU. Salinity values are listed in **Table 4** in the appendix.

Temperatures

As the temperature was measured every 10 cm along the cores exactly where the cores have been cut (**Table 4**, appendix), average temperature values are calculated from the top and bottom depths of 10 cm sample pieces. **Figure 5** (middle) depicts the average temperature values for Polar Fox Lagoon. For both cores, the temperature ranged from –15.1 °C (first 10 cm) to values about –0.6 °C (bottom depths), with mean values of –6.24 °C (core 31) and –6.73 °C (core 32) (**Table 2**). The temperature of both ice cores increased with depth. Temperatures warmer than –5 °C were recorded at depths ≥ 60 cm for core 31 and ≥ 120 cm for core 32, whereas temperatures warmer than –1.5 °C occurred in depths ≥ 150 cm for both cores.

Dissolved organic carbon

The DOC concentrations for core 31 and 32 of the Polar Fox Lagoon also followed a similar pattern in **Figure 5** (right). DOC concentrations varied in the upper portion of the ice cores and showed an increase with depth until the measured bottom depth. From 10 - 40 cm, concentrations ranged between 1.05 mg L^{-1} and 3.04 mg L^{-1} (core 31) and from 0.66 mg L^{-1} to 3.31 mg L^{-1} for the depths from 0 - 30 cm (core 32) (**Figure 5**, right). The concentrations were between 0.66 mg L^{-1} and 3.55 mg L^{-1} for both cores, with a mean value of 2.34 mg L^{-1} (core 31) and 2.66 mg L^{-1} (core 32) (**Table 2**).

Table 2: Table with mean [Min. – Max.] values for the analyzed hydrochemical parameters. For an overview and better comparability listed by all cores, Tiksi Bay (27-30) and Polar Fox Lagoon (31-32).

Core	$\delta^{18}O$ (‰)	δD (‰)	d-excess (‰)	EC (µS cm^{-1})	Temp. (°C)	DOC (mg L^{-1})	Cl^- (mg L^{-1})	SO_4^{2-} (mg L^{-1})
27	–15.6	–120	4.69	1186	–4.65	2.03	320	56.9
	[–16.7 - –14.7]	[–129 - –114]	[3.50 - 5.40]	[340 - 1724]	[–7.25 - –1.8]	[1.47 - 2.93]	[83.2 - 463]	[16.8 - 84.8]
28	–15.7	–120	5.10	1448	–3.63	1.99	388	68.7
	[–16.7 - –15.1]	[–128 - –116]	[4.40 - 5.70]	[414 - 2065]	[–6.45 - –1.5]	[1.00 - 2.45]	[106 - 567]	[17.7 - 98.7]
29	–15.7	–121	5.10	1157	–3.78	1.72	310	53.5
	[–16.7 - –15.1]	[–128 - –116]	[4.40 - 5.60]	[509 - 1485]	[–7.25 - –1.8]	[1.21 - 2.10]	[128 - 406]	[25.8 - 69.9]
30	–15.7	–120	5.09	129	–4.85	1.92	348	60.4
	[–16.7 - –15.2]	[–128 - –116]	[4.60 - 5.60]	[445 - 1731]	[–7.05 - –2.67]	[1.04 - 2.36]	[114 - 472]	[19.0 - 82.1]
31	–16.2	–123	5.88	1933	–6.24	2.66	499	82.9
	[–17.1 - –15.2]	[–130 - –116]	[4.60 - 7.60]	[101 - 3630]	[–12.2 - –2.10]	[1.05 - 3.55]	[23.4 - 936]	[5.64 - 149]
32	–16.2	–123	6.04	2011	–6.73	2.34	521	85.5
	[–17.1 - –15.0]	[–129 - –114]	[3.90 - 8.70]	[102 - 3520]	[–15.1 - –0.6]	[0.66 - 3.31]	[24.6 - 908]	[4.56 - 142]

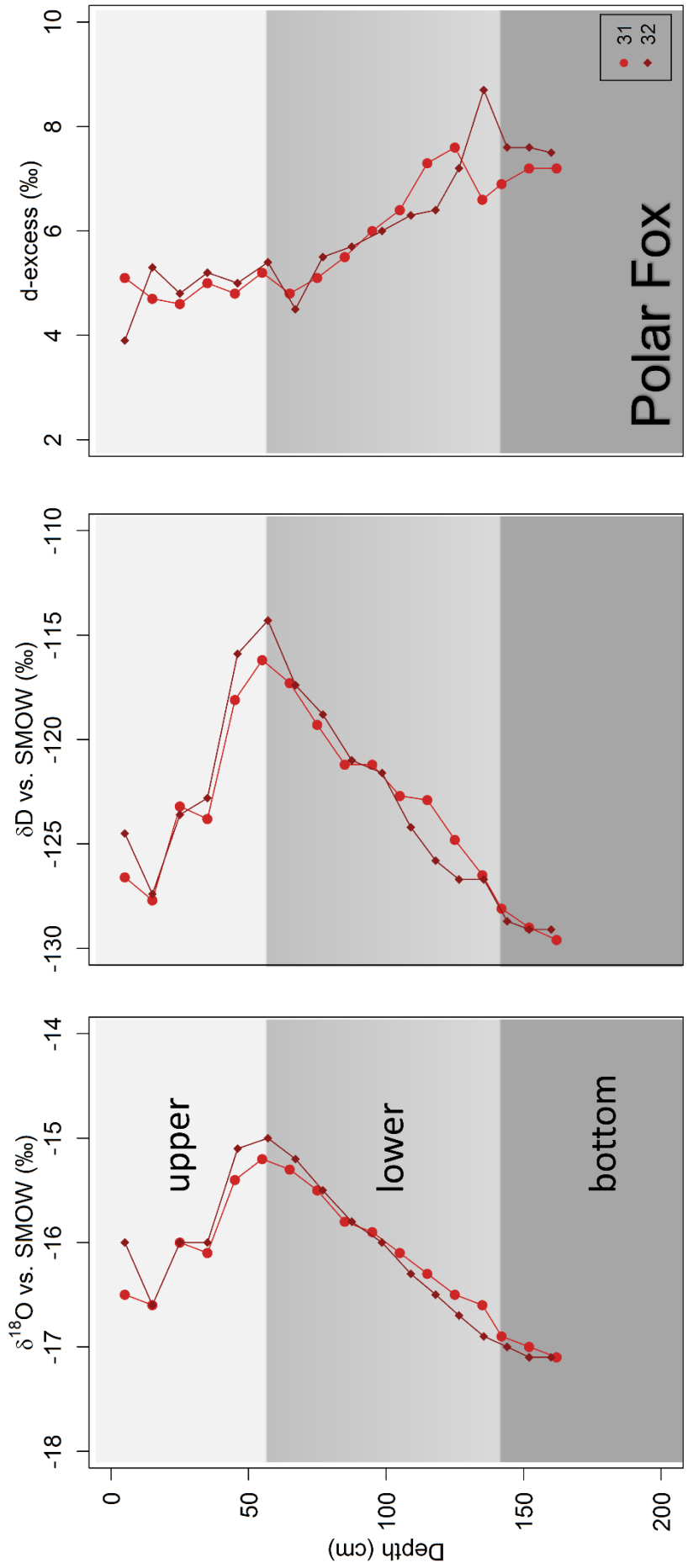

Figure 4: Vertical distribution of $\delta^{18}O$ (left), δD (middle) and d-excess (right) for the ice cores 31 (red circles) and 32 (dark red diamonds) of Polar Fox Lagoon. The water depth beneath the ice were: 2.81 m (core 31) and: 2.61 m (core 32) (Boike et al., (eds), in prep.). Note the different scale of the x-axes.

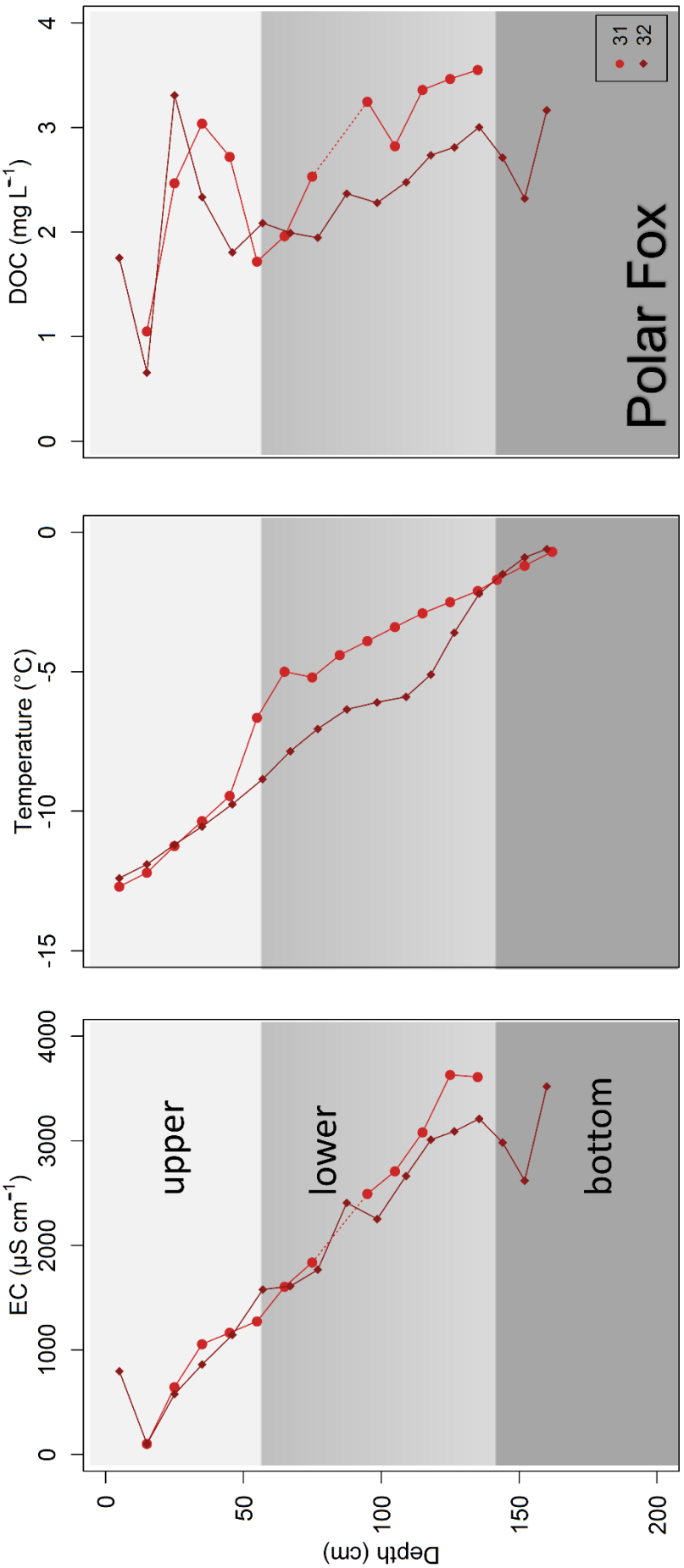

Figure 5: Vertical distribution of EC (left), Temperature (middle) and DOC (right) for the ice cores 31 (red circles) and 32 (dark red diamonds) of Polar Fox Lagoon. The water depths beneath the ice were: 2.81 m (core 31) and 2.61 m (core 32) (Boike et al., (eds), in prep.). The dotted line (core 31) indicates missing 10 cm in the middle of the core for EC and DOC.

Anions

The EC indicated a higher total ion content in the lower portion of the ice cores (> 3000 µS cm^{-1} at the depth > 110 cm). **Figure 6** shows concentrations of chloride (Cl^-) and sulfate (SO_4^{2-}). The concentrations of Cl^- and SO_4^{2-} showed the same trend among each other and the EC, therefore they do not indicate a change by other processes. The concentrations for both cores were comparable and ranged from 23.4 mg L^{-1} to 936 mg L^{-1} for Cl^- and 4.56 mg L^{-1} to 149 mg L^{-1} for SO_4^{2-} (**Table 2**).

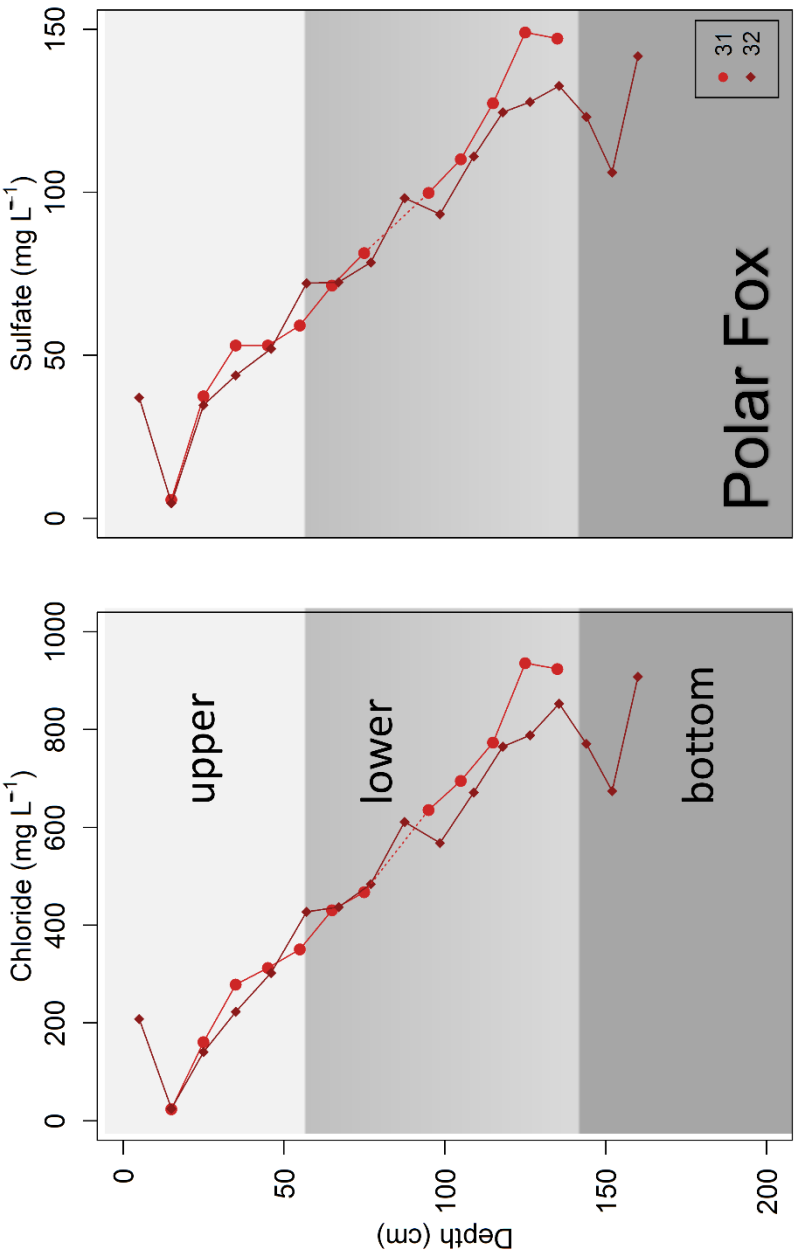

Figure 6: Vertical distribution of Chloride (left) and Sulfate (right) for the ice cores 31 (red circles) and 32 (dark red diamonds) of Polar Fox Lagoon. The water depths beneath the ice were: 2.81 m (core 31) and 2.61 m (core 32) (Boike et al., (eds), in prep.). The dotted line (core 31) indicates missing 10 cm in the middle of the core. Note the different scale of the x-axes

4.3 Hydrochemistry in the ice of Tiksi Bay

Stable water isotopes

For the four cores of the Tiksi Bay transect, $\delta^{18}O$ and δD values ranged from –16.7 ‰ to –14.7 ‰ and –128 ‰ to –114 ‰, respectively (**Table 2**). The stable water isotopes were in the same range as the $\delta^{18}O$ and δD values of Polar Fox Lagoon (see section 4.2), with a slight offset to heavier values. However, variations of stable isotopes with depth in the ice cores of Tiksi Bay were relatively similar to each other and changed in the upper and lower portion (**Figure 7**). While the values in the upper portion (until approximately 80 - 90 cm) were quite stable, except for the top of the ice, values decreased in the lower portion (> 80 - 90 cm). Between 10 – 20 cm and the middle of each core, the $\delta^{18}O$ and δD values were almost stable for all cores. In the upper portion the mean values (± standard deviation) are –15.0 ± 0.2 ‰ and –115.4 ± 1.1 ‰ (10 - 20 cm to 70 - 80 cm, core 27), as well as –15.2 ± 0.1 ‰ and –116.4 ± 0.4 ‰ (10 – 20 cm to 51 - 60 cm, core 28), –15.3 ± 0.2 ‰ and –117.5 ± 1.4 ‰ (10 - 20 cm to 70 - 80 cm, core 29) and –15.3 ± 0.1 ‰ and –117.6 ± 0.9 ‰ (between 0 - 10 cm and 80 - 88 cm core 30).

At the top of the ice, from 0 - 10 cm to 10 - 20 cm, the $\delta^{18}O$ and δD values increased slightly. In core 27 and 28, the values increased from –15.3 ‰ to –14.9 ‰ and –15.7 ‰ to –15.2 ‰ (change of 0.4 ‰ and 0.5 ‰) for $\delta^{18}O$, as well as from –118.6 ‰ to –115.0 ‰ and –120.8 ‰ to –116.8 ‰ (change of 3.6 ‰ and 4 ‰) for δD. There is a similar but smaller increase in core 29 (from –15.5 ‰ to –15.2 ‰ and –119.9 ‰ to –116.7 ‰ (for $\delta^{18}O$ and δD, respectively). The values were also stable at the top of the ice core 30 (from–15.3 ‰ to –15.2 ‰ and from –117.4 ‰ to –117.0 ‰, for $\delta^{18}O$ and δD, respectively).

In all cores, $\delta^{18}O$ and δD values decreased in the lower portion of the ice, from mid-core downward. While the water isotopic components of core 27 and 30 started to decrease from a depth of 80 - 90 cm, the $\delta^{18}O$ and δD values of core 28 and 29 began to decrease from 90 - 100 cm and 70 - 80cm respectively. The values were lowest in each case at the bottom of the ice cores. Core 27, the longest core and furthest from the shore, had a slightly larger range for $\delta^{18}O$ and δD values than the other cores (**Table 2**).

The d-excess also varied slightly more at core 27. Generally the d-excess was was quite stable with a range from 3.5 ‰ to 5.7 ‰ for all four cores (**Table 2**). Inter-core variability was larger in the upper portions of the cores, whereas all cores had a value of 5.5 ± 0.1 ‰ at the ice-water interface. For the cores of Tiksi Bay, no strong trend of the d-excess with depth along the cores was visible (**Figure 7**, right).

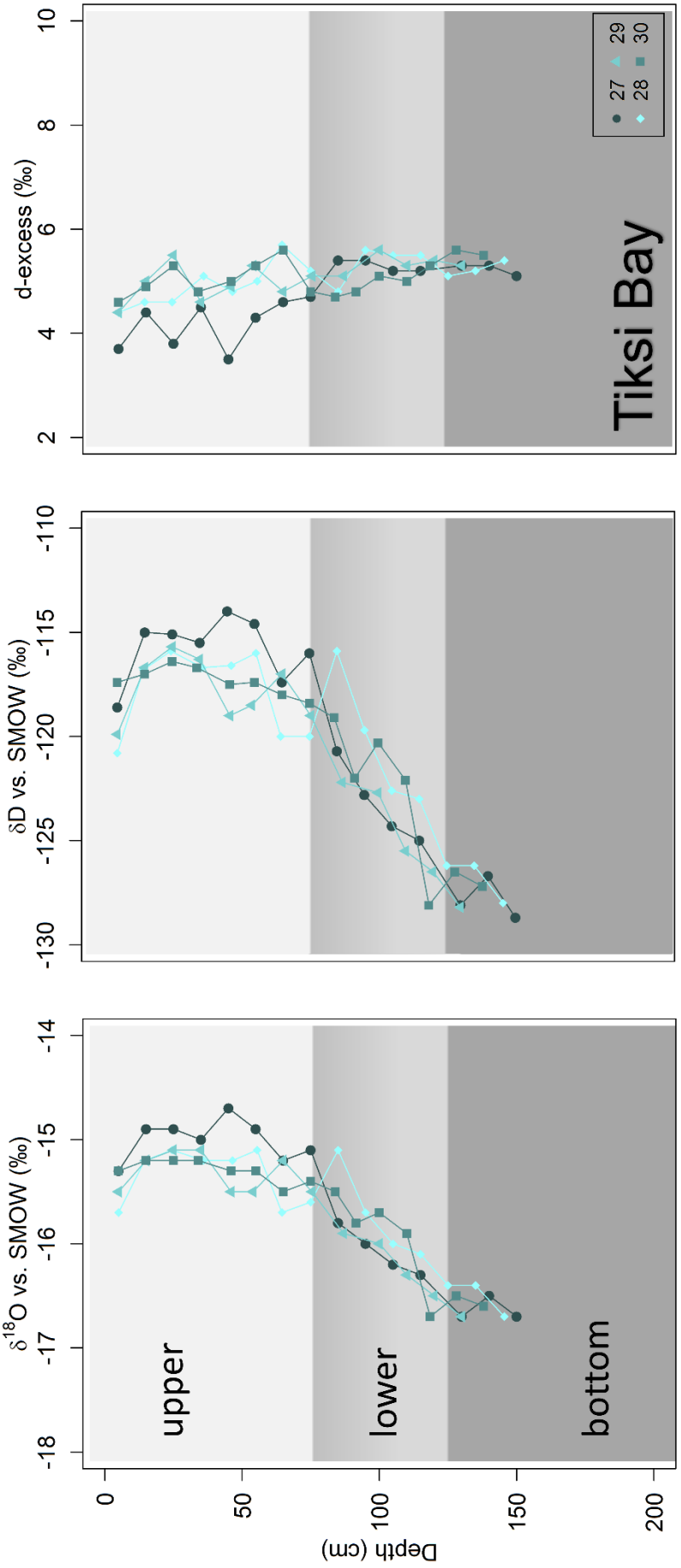

Figure 7: Vertical distribution of $\delta^{18}O$ (left), δD (middle) and d-excess (right) for the ice cores 27 (dark blue circles), 28 (blue-green diamonds), 29 (light blue triangles) and 30 (blue squares) of Tiksi Bay. The water depths beneath the ice were: 2.84 m (core 30), 3.87 m (core 29), 3.3 m (core 28) and 4.21 m (core 27) (Boike et al., (eds), in prep). Note the different scale of the x-axes.

Electrical conductivity and salinity

The transect of Tiksi Bay indicated EC values from 414 µS cm^{-1} to 2065 µS cm^{-1} for all cores (**Table 2**). All four cores showed a similar trend: the EC mainly increased with depth in the upper portion (until approximately 80 - 90 cm), whereas in the lower portion of the cores (> 80 - 90 cm) the EC decreased (**Figure 8**, left). At the bottom of all cores, the last 20 cm or 30 cm, the decrease is about 800 µS cm^{-1} or even greater (**Figure 8**, left and **Table 4**, appendix).

In the depths from 10 - 20 cm to ~40 - 50 cm, the EC increased from 1064 µS cm^{-1} to 1724 µS cm^{-1} (core 27) and from 1304 µS cm^{-1} to 2065 µS cm^{-1} (core 28). For core 29 and 30, the EC increased from 1111 µS cm^{-1} to 1485 µS cm^{-1} and from 1581 µS cm^{-1} to 1731 µS cm^{-1}, respectively between 0 - 10 cm and 40 - 50 cm. The EC decreased slightly from 1724 µS cm^{-1} to 1460 µS cm^{-1} (core 27, 40 - 50 cm to 80 - 90 cm), from 2065 µS cm^{-1} to 1238 µS cm^{-1} (core 28, 42 - 51 cm to 90 - 100 cm), from 1485 µS cm^{-1} to 1455 µS cm^{-1} (core 29, 42 - 50 cm to 71 - 80 cm), and from 1731 µS cm^{-1} to 1400 µS cm^{-1} (core30, 42 - 50 cm to 80 - 88 cm). In the lower portion of the ice cores, the EC was lower than 900 µS cm^{-1} (**Figure 8**, left and **Table 4**, appendix).

The salinity was higher than 0.5 PSU in the depths between 10 - 20 cm to 80 - 90 cm (core 27), 10 – 20 cm to 90 - 100 cm (core28), 10 - 20 cm to 71 - 80 cm (core 29) and 10 - 20 cm to 80 - 88 cm (core 30). Salinity values lower than 0.5 PSU were found at depths from 90 - 100 cm to 110 - 120 cm (core 27), 100 - 110 cm and 110 - 121 cm (core 28), 80 - 95 cm and 95 – 105 cm (core 29), and 88 - 95 cm to 105 - 115 cm (core30). Salinity values higher than 1 PSU occurred only at core 28, between 30 - 42 cm to 51 - 60 cm. Salinity values are listed in **Table 4**, appendix.

Temperature

Ice temperature ranged from values warmer than –8 °C (first 10 cm) to values about –1 °C in upper and lower portion of the cores (**Table 2**). The temperature for all ice cores of Tiksi Bay increased with depth, but for core 28 the temperature decreased slightly again in the last 30 cm. **Figure 8** (middle) shows the average temperature values for Tiksi Bay. Temperatures were warmer than –5 °C at depths ≥ 50 cm (core 27), ≥ 42 cm (core 28), ≥ 30 cm (core 29) and ≥ 60 cm (core 30). Ice was warmer than or equal to –1.5 °C at depths ≥ 125 cm (core27), ≥ 80 cm (core29), at 90-100 cm (core 28) and ≥ 123 cm (core 30).

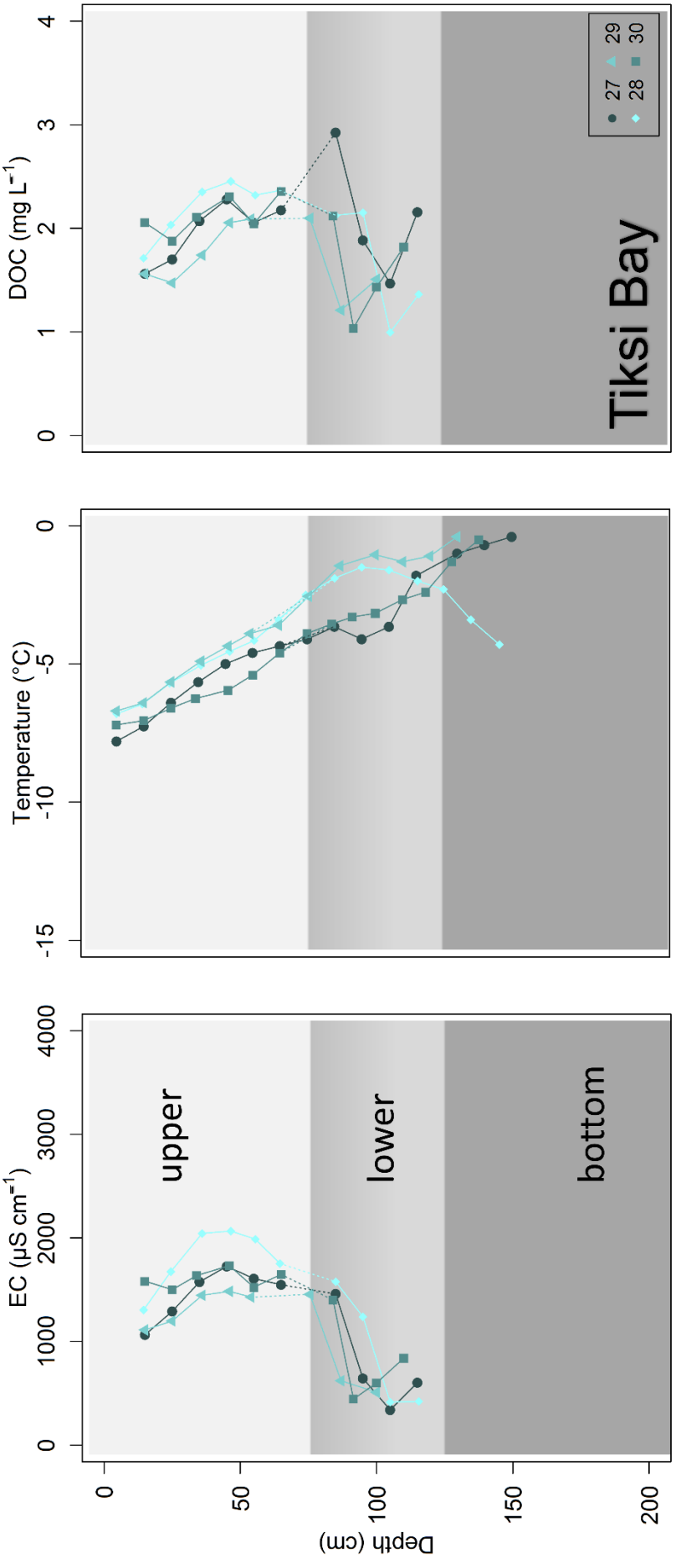

Figure 8: Vertical distribution of EC (left), Temperature (middle) and DOC (right) for the ice cores 27 (dark blue circles), 28 (blue-green diamonds), 29 (light blue triangles) and 30 (blue squares) of Tiksi Bay. The water depths beneath the ice were: 2.84 m (core 30), 3.87 m (core 29), 3.3 m (core 28) and 4.21 m (core 27) (Boike et al., (eds), in prep). The dotted lines indicate the missing 10 cm in the middle of the cores.

Dissolved organic carbon

The DOC concentration of the four cores ranged from 1.00 mg L^{-1} to 2.93 mg L^{-1} (**Table 2**). The concentrations increased slightly with depth in the upper portion of the cores. At the lower portion the concentrations decreased, but in the bottom depths they increased again. **Figure 8** (right) shows the DOC profile of Tiksi Bay.

Core 27 showed increased DOC concentrations in the depths between 10 - 20 cm and 80 - 90 cm from 1.56 mg L^{-1} to 2.93 mg L^{-1}, values increased from 1.71 mg L^{-1} (10 - 19 cm) to 2.45 mg L^{-1} (42 - 51 cm) for core 28, where the DOC concentrations of core 29 increased from 1.56 mg L^{-1} (10 - 20 cm) to 2.10 mg L^{-1} (71 - 80 cm). The concentrations at core 30 ranged from 1.88 mg L^{-1} (20 - 30 cm) to 2.26 mg L^{-1} (60 - 70 cm). The concentrations of core 27 decreased from 2.93 mg L^{-1} (80 - 90 cm) to 1.47 mg L^{-1} (100 - 110 cm), for core 28 from 2.45 mg L^{-1} (42 - 51 cm) to 1.00 mg L^{-1} (100 - 110 cm), values for core 29 were lowest in the depths of 80 - 95 cm and 95 - 105 cm, with 1.21 mg L^{-1} and 1.51 mg L^{-1}, respectively. In the lowermost sample (110 - 120 cm), the concentration was greater (2.16 mg L^{-1} in core 27 and 1.36 mg L^{-1} in core 28). For core 30 the concentrations were greater in the lowest three samples (88 - 95 cm, 95 - 105 cm, and 105 - 115 cm), with values of 1.04 mg L^{-1}, 1.42 mg L^{-1} and 1.82 mg L^{-1}, respectively.

Anions

Concentrations for the whole cores ranged from 23.4 mg L^{-1} to 924 mg L^{-1} for Cl^- and from 4.6 mg L^{-1} to 147 mg L^{-1} for SO_4^{2-}. **Figure 9** shows the concentrations of Cl^- and SO_4^{2-} with depth. The pattern for both anions is the same: an increase in concentration with increasing depths. Both anions thus mirror the variations in EC.

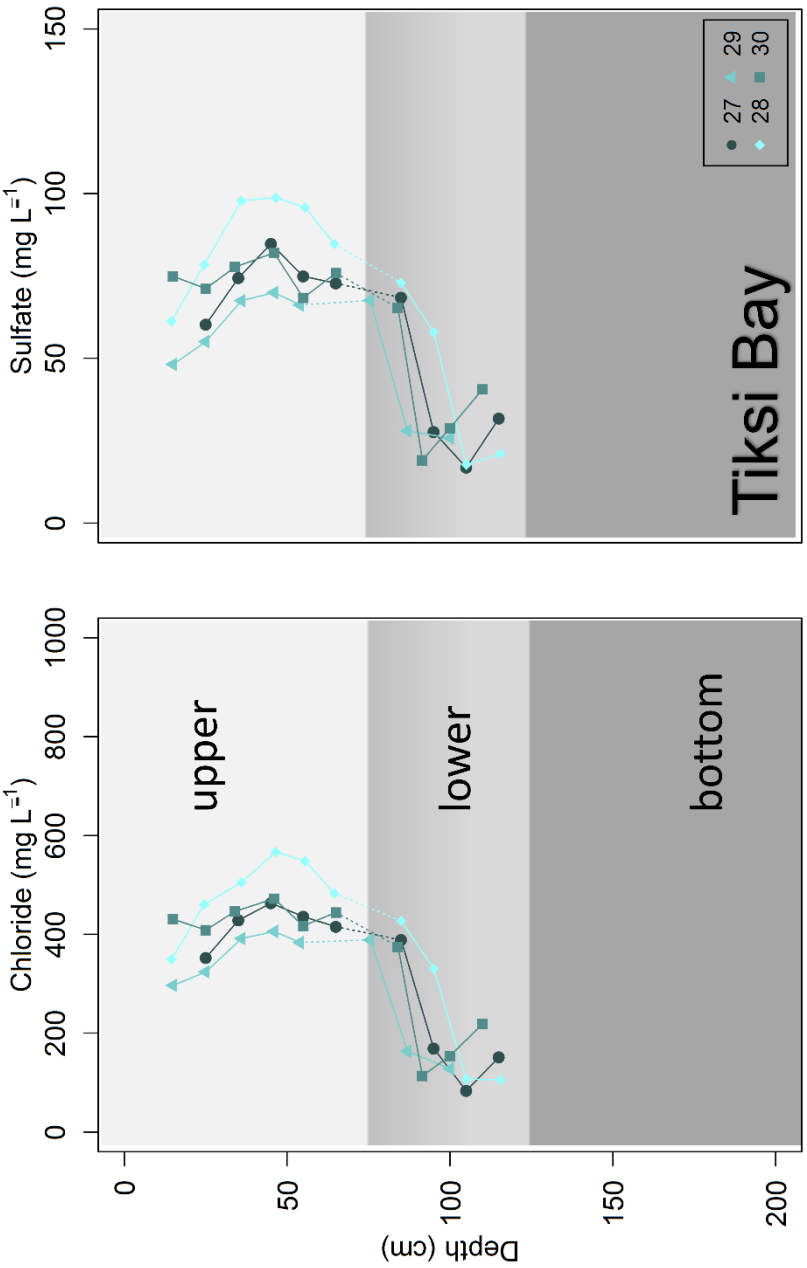

Figure 9: Vertical distribution of Chloride (left) and Sulfate (right) for the ice cores 27 (dark blue circles), 28 (blue-green diamonds), 29 (light blue triangles) and 30 (blue squares) of Tiksi Bay. The water depths beneath the ice were: 2.84 m (core 30), 3.87 m (core 29), 3.3 m (core 28) and 4.21 m (core 27) (Boike et al., (eds), in prep). The dotted lines indicates missing 10 cm in the middle of the cores. Note the different scale of the x-axes.

4.4 Methane in the ice of Polar Fox Lagoon

Dissolved methane concentrations

CH_4 concentrations for Polar Fox covered a wide range, with values from 2.59 nM to 539 nM (**Table 3**). The concentrations in the two ice cores were similar. **Figure 10** (left) shows the distribution of CH_4 concentrations with depth. In the upper 50 cm of the ice, the CH_4 concentrations were more variable than in the rest of the ice cores. In the lower portion of the cores, the concentrations were consistently lower than in the upper portion. In the bottom portion, where only data for core 32 exist, the concentrations increased.

At depths from 10 - 20 cm to 30 - 40 cm, concentrations were between 85.6 nM (10 - 20 cm) and 194 nM (20 - 30 cm) (core 31) and ranged from 20.1 nM (10 - 20 cm) to 161 nM (0 - 10 cm) for the depths from 0 - 10 to 20 - 30 cm (core 32). The CH_4 concentrations decreased from 194 nM (20 - 30 cm) to 3.02 nM (60 - 70 cm) for core 31 and from ~129 nM (20 - 30 cm and 30 - 40 cm) to 2.89 nM (52 - 62 cm) for core 32. Generally lower concentrations occurred between 3.02 nM (60 - 70 cm) and 7.26 nM (70 - 80 cm) for core 31 as well as between 2.59 nM (62 - 72 cm) and 6.84 nM (131 - 140 cm) for core 32 in the lower portion of the ice. Concentrations increased from 10.3 nM to 539 nM in the last three measured depths of core 32 (140 - 148 cm to 156 - 164 cm).

Stable carbon isotopic signature of methane

The $\delta^{13}C_{CH4}$ values ranged from –79.7 ‰ to –31.8 ‰ for both cores (**Table 3**). The two cores indicated a similar pattern, with carbon isotopes more enriched in ^{13}C in the lower portion of the cores than in the upper portion (**Figure 10**, right). In the bottom depths, where measurements for core 32 exist, the stable $\delta^{13}C_{CH4}$ values decreased. The pattern is similar but inverse to the CH_4 concentrations. The $\delta^{13}C_{CH4}$ most depleted in ^{13}C occurred at the top of the ice cores, with values from –77.5 ‰ (10 - 20 cm) to –57.1 ‰ (30 - 40 cm) for core 31 and –79.7 ‰ (0 - 10 cm) to –63.0 ‰ (30 - 40 cm) for core 32 in the upper 40 cm. The $\delta^{13}C_{CH4}$ values increased between 20 - 30 cm to 90 - 100 cm, from –77.0 ‰ to –31.8 ‰ (core 31) and between 30 - 40 cm to 72 - 82 cm, from –63.0 ‰ to –38.0 ‰ (core 32). In the lower portion of the cores, where the lower CH_4 concentrations were detected, the values ranged from –31.8 ‰ (90 - 100 cm) to –47.9 ‰ (50 - 60 cm) between 40 - 50 cm and 130 - 140 cm for core 31; and from –38.0 ‰ (72 - 82 cm) to –48.0 ‰ (131 - 140 cm) between 52 - 62 cm and 131 - 140 cm for core 32. In the last three measured depths of core 32 (between 140 - 148 cm and 156 - 164 cm), an increase towards higher isotopic values, enrichment in ^{12}C, with depth is reflected in the values from –52.2 ‰ to –69.5 ‰. But the $\delta^{13}C_{CH4}$ is with –48.0 ‰ already slightly increased in the depth before (131 - 140 cm).

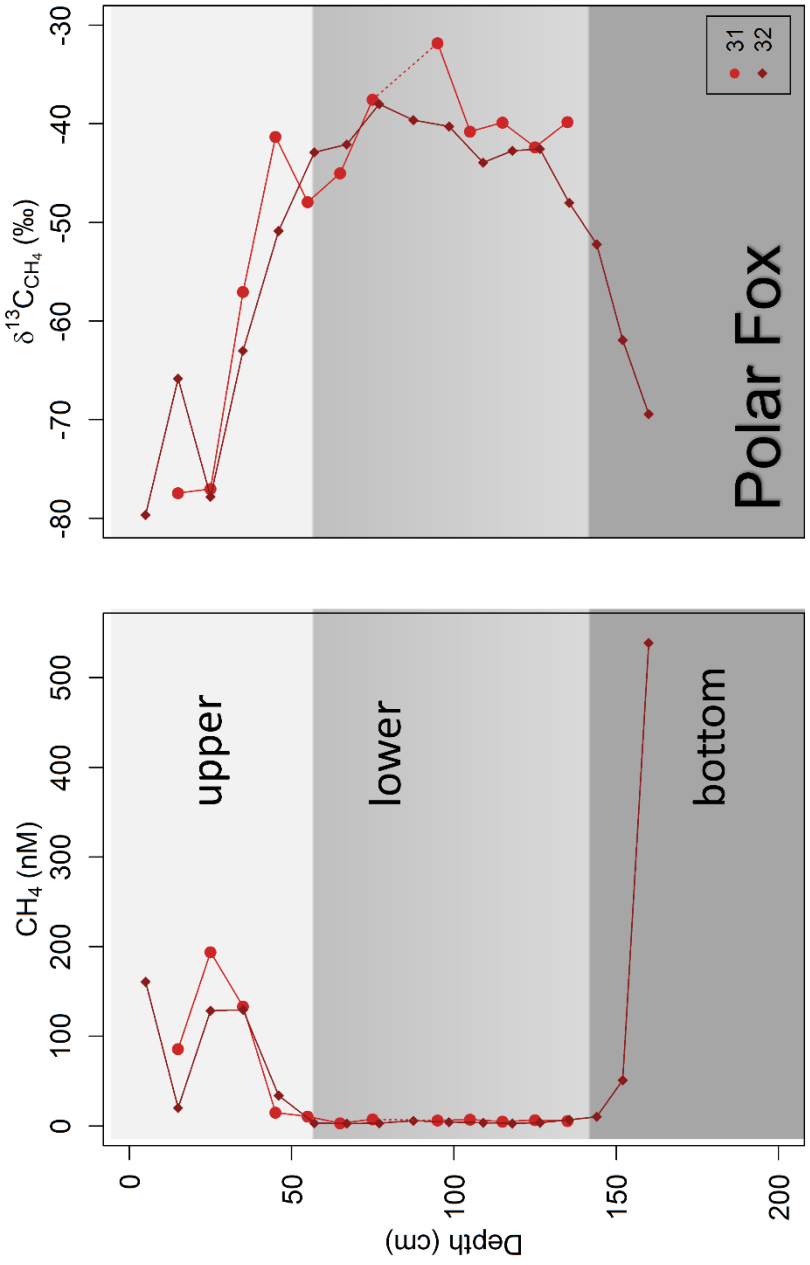

Figure 10: Vertical distribution of dissolved methane concentrations (left) and carbon isotopic signatures of methane (right) for the ice cores 31 (red circles) and 32 (dark red diamonds) of Polar Fox Lagoon. The water depth beneath the ice were: 2.81 m (core 31) and: 2.61 m (core 32) (Boike et al., (eds), in prep.). The dotted line (Core 31) indicates missing 10 cm in the middle of the core.

4.5 Methane in the ice of Tiksi Bay

Dissolved methane concentrations

The CH_4 concentrations of the cores from Tiksi Bay were with values from 3.48 nM to 8.44 nM in a small range compared to Polar Fox Lagoon (**Table 3**). **Figure 11** (left) presents the CH_4 concentrations for the ice cores of Tiksi Bay. The concentrations were quite stable in the upper portion of the ice cores. No trend was visible in the depths until ~ 80 - 90 cm, but all cores indicated a trend of decrease of CH_4 concentrations from the depth above 80 - 90 cm, except core 28, where the concentrations decreased from a depth of 100 - 110 cm. For core 27 and 30, the CH_4 concentration slightly increased in the last measured depth again, whereas the concentration of core 29 further decreased.

For core 27, concentrations ranged from 5.10 nM (40 - 50 cm) to 6.11 nM (60 - 70 cm) in the depths between 10 - 20 cm and 60 - 70 cm and decreased to values of 3.69 nM and 3.85 nM (90 - 100 cm and 100 - 110 cm, respectively). The concentration in the last measured depth is with 4.50 nM (110 - 120 cm) slightly higher again.

The concentrations of core 28 were between 5.47 nM (30 - 42 cm) and 6.75 nM (60 - 69 cm) in the depths from 10 - 20 cm to 90 - 100 cm. In the depths of 100 cm to 121 cm, the concentration decreased with values of 5.14 nM (100 - 110 cm) and 4.97 nM (110 - 121 cm).

At core 29, concentrations from 5.43 nM (20 - 30 cm) to 7.21 nM (10 - 20 cm) occurred in the depths between10 - 20 cm and 70 - 80 cm. The concentration decreased in the depths of 80 - 95 cm and 95 - 105 cm to 4.06 nM and 3.48 nM, respectively.

Core 30 showed concentrations from 6.55 nM to 8.44 nM in the depths between 10 - 20 cm and 60 - 70 cm. In the depths from 80 - 88 cm to 95 - 105 cm, the concentrations decreased to 6.05 nM. In the last measured depth of 110 - 115 cm, the concentration increased slightly to 7.64 nM.

Stable carbon isotopic signature of methane

The $\delta^{13}C_{CH4}$ values for the cores of Tiksi Bay were with values ranging from –51.9 ‰ to –36.9 ‰ also in a smaller range than the $\delta^{13}C_{CH4}$ values for the cores of Polar Fox Lagoon (**Table 3**). **Figure 11** (right) shows the $\delta^{13}C_{CH4}$ values for the ice cores of Tiksi Bay. The trend is similar but inverse to the CH_4 concentrations from Tiksi Bay, $\delta^{13}C_{CH4}$ values were almost stable in the upper portion of the cores. From the depth of 80 - 90 cm, the $\delta^{13}C_{CH4}$ values for the cores 27, 28 and 30 was higher in the lower portion of the cores and decreased with depth.

At core 27, in the depths between 10 - 20 cm and 60 - 70 cm the values were between –51.9 ‰ (50 - 60 cm) and –49.4 ‰ (10 - 20 cm), whereas in the depths from 80 - 90 cm to 110 - 120 cm

higher values occurred. The $\delta 13C_{CH4}$ values in these depths ranged from –48.1 ‰ (110 - 120 cm) to –36.9 ‰ (80 - 90 cm), but decreased with depth.

For core 28, the values were in a range from –48.3 ‰ (42 - 51 cm) to the highest value of –39.2 ‰ (90 - 100 cm). From the depths of 90 - 100 cm to 100 - 121 cm the values range from –39.2 ‰ to –44.6 ‰ and decreased with depth.

Core 29 did not show a clear trend in the $\delta 13C_{CH4}$ values. The lowest value was –50.9 ‰ (30 - 42 cm) and the highest value –44.7 ‰ ± 0.1 ‰ (50 - 58 cm, 42 - 50 cm, and 95 - 105 cm).

For core 30, the value ranged from –50.9 ‰ to –44.6 ‰ in the depths from 20 - 30 cm to 60 – 70 cm. With values between –43.7 ‰ and –40.2 ‰ the $\delta 13C_{CH4}$ was enriched in ^{13}C in depths between 80 - 88 cm and 95 - 105 cm. In the depth of 105 - 115 cm, the $\delta 13C_{CH4}$ values decreased to –49.6 ‰ again.

Table 3: Table with mean [Min –Max] values for the analyzed CH_4 concentrations and $\delta^{13}C_{CH4}$ values. Listed by **all** cores, Tiksi Bay (27-30) and Polar Fox lagoon (31-32).

Core	**CH_4 (nM)**	**$\delta^{13}C_{CH4}$ (‰)**
27	5.11 [3.69 - 6.11]	–46.8 [–51.9 - –36.9]
28	5.93 [4.97 - 6.75]	–45.0 [–48.3 - –39.2]
29	5.79 [3.48 - 7.21]	–46.8 [–50.9 - –44.8]
30	7.23 [6.05 - 8.44]	–45.6 [–50.9 - –40.2]
31	39.9 [3.02 - 194]	–48.2 [–77.5 - –31.8]
32	65.2 [2.59 - 539]	–53.0 [–79.7 - –38.0]

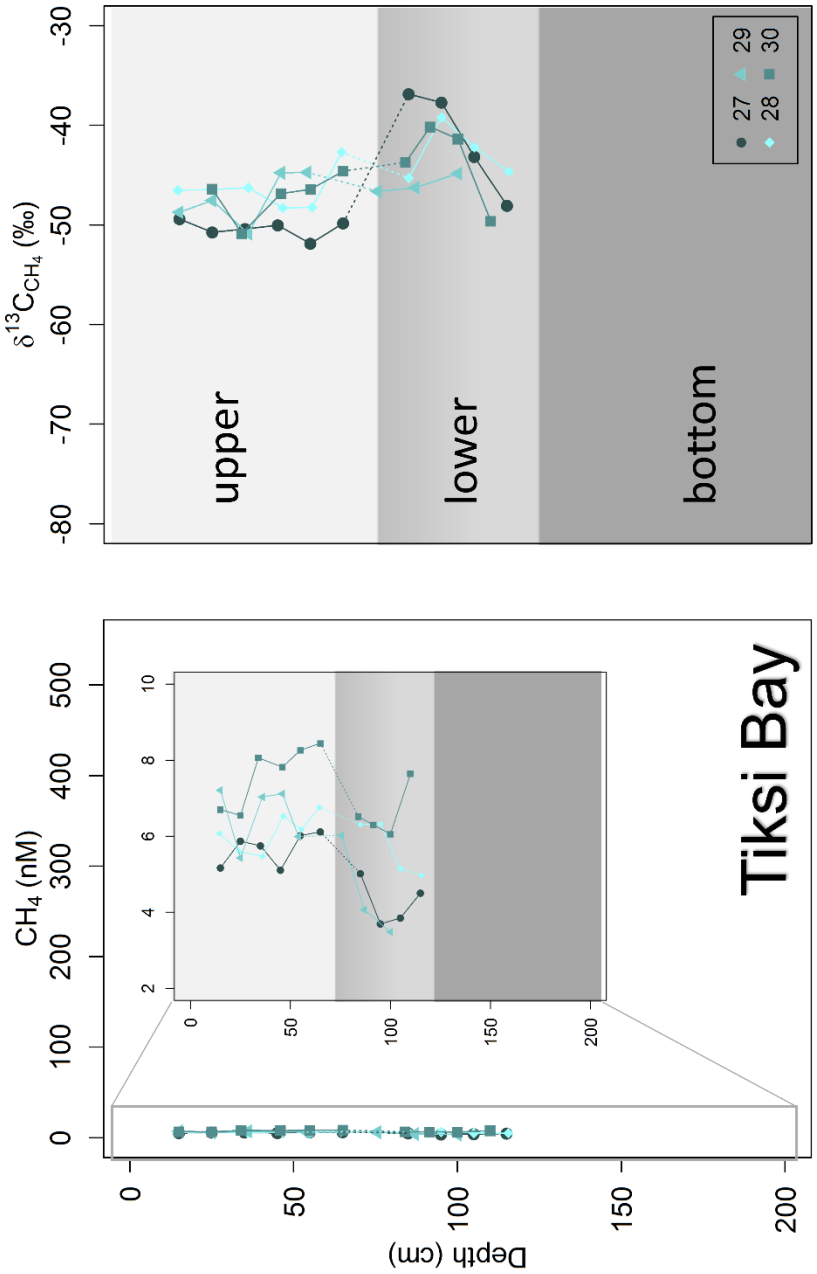

Figure 11: Vertical distribution of dissolved methane concentrations (left) and carbon isotopic signatures of methane (right) for the ice cores 27 (dark blue circles), 28 (blue-green diamonds), 29 (light blue triangles) and 30 (blue squares) of Tiksi Bay. A plot with a smaller scale for the methane concentrations (from 2-10 nM) is integrated to demonstrate smaller changes of the methane concentrations. The scale of 0-550 nM was chosen for a better comparability between Tiksi Bay and Polar Fox. Dotted lines indicate missing 10 cm in the middle of the core. Note the different scale of the *x*-axes.

5 Discussion

This study focuses on the floating ice cover of two water bodies, one of which is a semi-closed water body (Polar Fox Lagoon, no winter exchange of water with other water bodies) and the other open (Tiksi Bay, perennially connected to Buo Khaya Bay and the Arctic Ocean). The ice cores of this study offer a record from approximately October 2016, when the ice started to form, until the beginning of April 2017, when the ice cores were taken. Therefore, the data are influenced by temporal changes from the beginning of the ice formation over the winter period until the time when the ice cores were collected. These changes were presumably dependent on processes in the water before and during freezing, as well as processes in the ice after freezing. Since the ice grows by freezing at the ice-water interface, the ice cores record changes in the water along their length, cores were about 150 ± 15 cm long. The results presented here use the ice cores as an archive for winter ice-water processes. In the following, processes taking place during freezing and processes changing the concentration of CH_4 enclosed therein will be discussed in detail for both, the semi-closed and open system.

First, freezing and hydrochemical changes coupled to the freezing are discussed. The stable water isotopic composition and the salinity were used to analyse these processes. Second, the CH_4 distribution in the ice is discussed in the context of processes during freezing and modifications after the freezing. This part of the discussion is based on the CH_4 concentrations and the $\delta^{13}C$ values in the ice cores. Finally, the semi-closed (Polar Fox Lagoon) and open system (Tiksi Bay) are compared to emphasize the main similarities and differences in terms of the discussed processes.

5.1 Water composition during freezing

The freezing process is driven and influenced by air and water temperatures, inflow or circulation of water and the growing ice thickness, which changes the water volume and the composition of the water underneath the ice (Adams & Lasenby, 1985). A snow layer on the ice can slow the freezing process by insulating the underlying ice from the cold air (Sturm & Massom, 2010). For energy and gas fluxes, it is important to distinguish between bedfast ice (ice frozen to the ground) and floating ice (Antonova et al., 2016).

Variations in the water isotopic composition and the salinity are expected to be conservative and reflect differences in the hydrological processes, such as a change in water masses and water inflow or outflow (Morimoto et al., 2010). Differences in isotopic fractionation are also visible in the water isotopic composition (e.g. O'Neill, 1968).

A semi-closed system – Polar Fox Lagoon

The analyzed ice cores of Polar Fox Lagoon were floating ice, with similar water depth remained beneath the ice (core 31: 2.81 m, core 32: 2.61 m) (Boike et al., (eds), in prep.). As Polar Fox is a thermokarst lagoon located in a permafrost region (see chapter 2), this water body is expected to be unaffected by groundwater inflow during winter. Besides a talik (unfrozen sediments under the lagoon due to heat transfer from the water), the ground surrounding the lagoon was frozen during winter (Schirrmeister et al., 2018). Polar Fox drains into Tiksi Bay through a wide, shallow and winding channel. Storm surges and high water events in the summer force sea water, driftwood and sediment into Polar Fox Lagoon (Overduin, 2018, personal communication). This channel, which is roughly 0.5 m deep where it exits the lagoon, no longer connects the lagoon to the bay during the winter when the ice in the channel freezes to the bed (bedfast ice). Thus, the lagoon changes from a semi-closed to a closed system at some point in the winter. In a closed system, the water body is isolated from water inflow or outflow. The timing when Polar Fox Lagoon changes to a closed water body depends on the rate of freezing and the depth of the channel and probably varies from year to year.

When freezing begins, the drainage channel still allows water exchange between the Lagoon and the Bay. This is reflected in the water isotopic composition. In depths between 30 and 60 cm in the ice, the isotopic signal of Polar Fox Lagoon ice clearly increased towards the isotopic signal of the water from the bay. The $\delta^{18}O$ value increased from –16 ‰ to –15 ± 0.2 ‰ and the δD value increased from –123.4 ± 0.2 ‰ to –115.2 ± 1 ‰, whereas the d-excess did not changed in the upper 60 cm of the ice (**Figure 4,** chapter 4). The electrical conductivity in the upper 30 cm (< 1000 µS cm^{-1}) is lower than the conductivity in the ice of the bay (**Table 4**, appendix), but reaches the conductivity of the bay at a depth of 50 - 60 cm.

Isotopic fractionation may also affect $\delta^{18}O$ and δD values. During freezing, the heavy isotopes are preferentially incorporated into the solid ice phase (Gibson & Prowse, 1999, 2002). If the reaction rate is constant (in this case phase change), equilibrium isotopic fractionation occurs (Gibson & Prowse, 1999). Gibson & Prowse (1999) summarized equilibrium fractionation, commonly expressed as isotopic separation factor, from other studies: experimental values of ε in freshwater systems are about 2.8 to 3.1 ‰ for oxygen (Suzuoki & Kimura, 1973; O'Neill, 1968) and 17.0 ‰ to 20.6 ‰ for hydrogen (Kuhn & Thürkauf, 1958; Arnason, 1969) at 0 °C and natural freezing rates (< 2 mm/hr). Isotopic fractionation is predicted to vary with the rate of freezing (Gibson & Prowse, 1999). The freezing rate for floating ice generally decreases with depth (Anderson, 1961). Thus, isotopic changes in the first 20 cm of Polar Fox with < 1 ‰ for oxygen and < 5 ‰ for hydrogen might be explained by variations in isotopic fractionation due

to freezing rate changes and are therefore lower than the changes given in the literature for equilibrium fractionation. I expect the freezing rate to change in the first 20 cm due to a rapid freezing of the first centimetres of the ice, when the water temperatures fall to the freezing point. The later formed ice is determined by slower freezing rates, especially after the ice is covered with snow. Furthermore, non-equilibrium processes during ice formation may affect isotopic variation (Suzuoki & Kimura, 1973). Which are also dependent on the freezing rate and the mixing rate of the water under the ice. An isotopic gradient is established in the water near the ice-water interface, if the freezing rate is high compared to the water mixing rate and results in non-equilibrium fractionation (Lehmann & Siegenthaler, 1991). Non-equilibrium fractionation can be further influenced by trapped liquid water during crystal growth (Suzuoki & Kimura, 1973). As these effects usually reduce the isotopic fractionation compared to equilibrium fractionation, fractionation effects are usually weaker under natural conditions than under experimental conditions.

In the lower portion of the ice, the data of this study showed a clear shift in the isotopic signal to decreasing values in the ice below 60 cm. The isotopic composition matches that of fractionation in a closed system (Gibson & Prowse, 1999). Freezing in a closed system leads to a reduction of water volume beneath the ice and a concentration of dissolved constituents, since further freezing results in the loss of liquid water. As the heavy isotopic species are preferentially incorporated into the ice phase, the remaining water in closed systems becomes more and more depleted in heavy isotopes (Gibson & Prowse, 2002). This causes a decrease in the $\delta^{18}O$ and δD values towards the bottom of the ice. This fractionation effect was also shown in the increased d-excess values. If d-excess values exceed 10 ‰, less than 50 % of the residual water is left (Lacelle, 2011). This was not the case for Polar Fox Lagoon, where the d-excess values were consistently lower than 10 ‰ (**Figure 4**, chapter 4). Polar Fox had a mean depth of about 1.5 m with lower depths towards the lake shore and greater depths in the interior of the lake. As the ice thickness was about 1.6 m I expect the outer lake area frozen to the bed and probably more than 50 % of the whole lagoon area to be frozen. But in the middle of the lagoon, where the cores were taken, water depth of 2.71 ± 0.1 m remained beneath the about 1.6 m thick ice. Considering this ratio of ice and water, more than 50 % of the water column is not froze in this area of the lake.

As freezing proceeds, the concentration of dissolved salts is demonstrated in the continuous increase of the electrical conductivity (EC) towards the bottom of the analyzed ice cores from Polar Fox, which increases the permeability of the ice (Cottier et al., 1999). The dissolved organic carbon (DOC), Cl^- and SO_4^{2-} concentrations increased in the lower portion of the ice as

well (**Figure 5**, **Figure 6,** chapter 4) and point to the accumulation of organic material and anions in the remaining water.

Figure 12 shows an $\delta^{18}O$ versus δD plot for Polar Fox Lagoon, with least squares best-fit linear regression lines for the upper and lower portions of the ice cores (semi-closed and closed system, respectively). The δD-$\delta^{18}O$ slope is characteristic of the freezing process (Souchez & Jouzel, 1984). Slope values in the range of 6 to 7.3 can be interpreted as freezing under equilibrium conditions (Lacelle, 2011). The samples of the lower portion of the ice, under totally closed system conditions, plots along a regression slope of 6.1 ($\delta D = 6.1\ \delta^{18}O–24.4$). In contrast, the samples of the upper portion of the ice, semi-closed system conditions, plot along a regression line of 8.1 ($\delta D = 8.1\ \delta^{18}O+7.2$) and indicate a different freezing process. As the upper freezing was influenced by mixing of the initial water with a different water mass, water from the bay, probably no equilibrium freezing occurred.

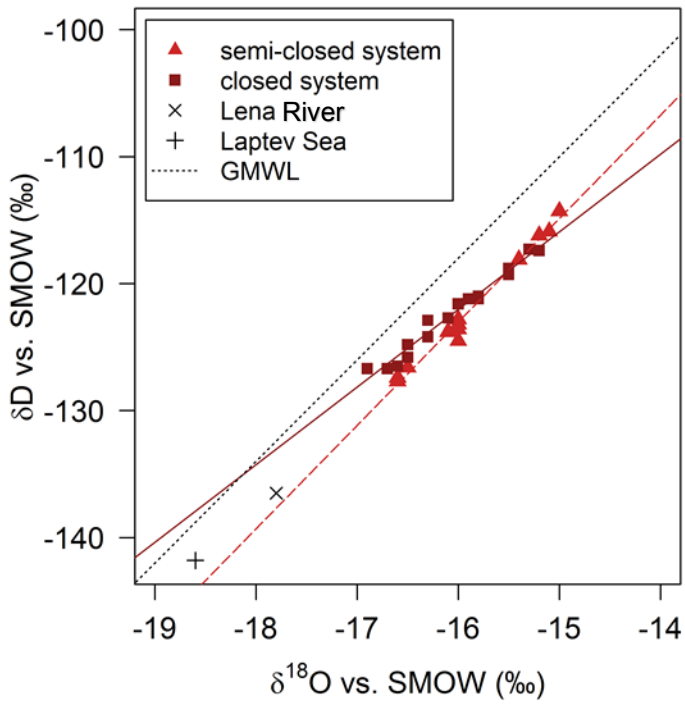

Figure 12: Isotope composition and linear regressions for Polar Fox Lagoon ice cores. Samples are classified as semi-closed (depths 0-60 cm, $\delta D = 8.1\ \delta^{18}O + 7.2$, r^2=0.98, n=10, red dashed line) or closed (depths 60-164 cm, $\delta D = 6.1\ \delta^{18}O$ -24.4, r^2=0.97, n=14, dark red solid line) Values for the Lena River (n=16) and Laptev Sea (n=6) are mean summer values (Meyer, 2018, personal communication). With the global meteoric water line (GMWL, $\delta D = 8 * \delta^{18}O + 10$; (Craig, 1961), black dotted line).

An open system – Tiksi Bay

In contrast to Polar Fox, Tiksi Bay is an open bay and characterized by the mixing of freshwater runoff from the Lena River and the surrounding catchment in spring and from Laptev Sea marine water. Lena water flushes into the bay during the spring floods, which occur on average

between May and July and constitute approximately 60 % of the annual discharge volume (Magritsky et al., 2018). It is likely that little Lena water flows into Tiksi Bay during the winter, since discharge volumes are smaller and the flow is restricted beneath the sea ice. The stable low-water season of Lena-runoff over winter starts in late October and reaches minimal water discharge in April (Alekseevskii et al.,2014; Magritsky et al., 2018). The differences in densities of Lena's comparatively warm freshwater discharge and cold Laptev seawater result in a stratified water column. Measurements along a profile across Tiksi Bay in summer 2016 show an increase of EC at about four meters depth (Overduin et al., 2017). The upper water layer in Tiksi Bay is therefore fresh and with low salinity in summer. The saline, dense seawater accumulates under the brackish, less saline and less dense water. The water column may become mixed through cooling or storms during fall (Janout et al., 2016).

Satellite images from SENTINEL Hub (2018) indicated that the ice of the bay started to form later than the ice of Polar Fox Lagoon (approximately at the end of October). As I expect bay water flashing into the lagoon in the first period of the freezing, caused by storm events or high waters, those events are expected to be reflected in the ice of Tiksi Bay as well. Storm events are expected to result in well mixing of the upper waters. In an open system, where the stable water isotopes circulate freely beneath the ice cover, the ice composition remains constant with depth (Gibson & Prowse, 1999). Appropriately, a stability of the water isotopic composition and salinity values is shown until a depth of approximately 80 - 90 cm, except at the top of the ice (**Figure 7, Figure 8,** chapter 4). The variation of the stable water isotopic signal at the top might be due to isotopic fractionation variant with a change of the freezing rate.

Surprisingly, an increased Lena river water proportion is indicated by the data in the lower portion of the ice (> 80 - 90 cm). The stable water isotope composition decreased to $\delta^{18}O$ and δD values of –16.7 ‰ and –128 ‰, with d-excess about 5.1 ‰ (Lena river water summer mean values were $\delta^{18}O$: –17.8 ± 0.03 ‰ and δD: –137 ± 0.3 ‰ with a d-excess of ~ 5.9 ‰ (Meyer, 2018, personal communication), simultaneously the EC, as well as Cl^- and SO_4^{2-} concentrations are decreased.

Figure 13 shows an $\delta^{18}O$ versus δD plot for Tiksi Bay, with regression lines for the upper and lower ice. The regression lines clearly demonstrate differences in the two portions of the ice. The samples of the upper portion of the ice, demonstrating open system freezing, plot along a regression slope of 6.9 ($\delta D = 6.9\ \delta^{18}O–11.9$), indicating equilibrium freezing (Lacelle, 2011). In contrast, the samples of the lower portion of the ice, open system influenced by water mixing, plot along a regression line of 7.9 ($\delta D = 7.9\ \delta^{18}O+3.7$). The exchange of the water below the

ice might have disturbed an equilibrium freezing process, as it changed the isotopic composition of the initial water.

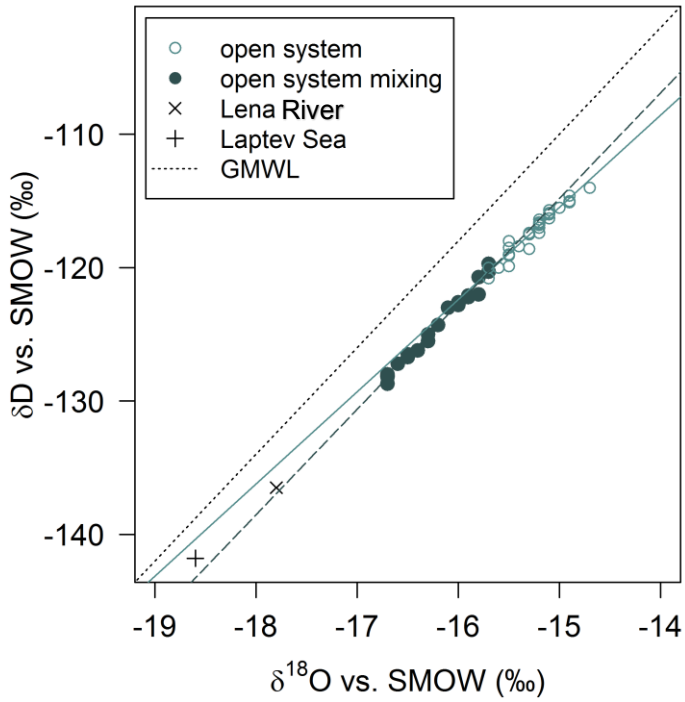

Figure 13: Isotope composition and linear regressions for Tiksi Bay ice cores. Samples are classified as open (depths ≤ 80-90 cm, δD = 6.9 δ18O -11.9, r^2=0.94, n=32, blue solid line) or open influenced by water mixing (depths > 80-90 cm, δD = 7.9 δ18O+3.7, r^2=0.99, n=22, dark blue dashed line) Values for the Lena River (n=16) and Laptev Sea (n=6) are mean summer values (Meyer, 2018, personal communication). With the global meteoric water line (GMWL, δD = 8 * $\delta^{18}O$ + 10; (Craig, 1961), black dotted line).

A comparison of Polar Fox and Tiksi Bay

Polar Fox Lagoon and Tiksi Bay clearly differ in their freezing processes. In both systems changes are shown between the upper and the lower portion of the ice. Polar Fox Lagoon was affected by water from Tiksi Bay in the first period of the winter, whereas later in winter, when the channel was frozen Polar Fox Lagoon resulted in a closed freezing system.

Tiksi Bay was a permanently open freezing system. Here, the processes are additionally influenced by water mixing indicated by an increase in the amount of freshwater during the advanced winter period.

5.2 Freezing processes, ice permeability and methane concentration in ice

At the beginning of the freezing period, when the ice cover is not totally closed, an exchange of gases between the water and the atmosphere is still possible (Bastviken et al., 2004). Later on, when the ice cover is totally closed, the ice is a physical barrier for gases (Parmentier et al., 2013). The gas exchange primarily depends on the permeability of the ice (Thomas, 2012). Hence, restricted gas exchange enhanced the uptake of CH_4 in lake ice during ongoing freezing.

Indeed, the ice, covering the two investigated water bodies (Polar Fox Lagoon and Tiksi Bay), is mostly supersaturated in CH_4 relative to the atmosphere, where the concentrations are almost 2 ppm (NOAA, 2018), which corresponds to a calculated equilibrium concentration of about 5 nM related to the temperature and salinity of the lagoon and bay water, calculated after Wiesenburg & Guinasso (1979).

CH_4 supersaturation in the ice might create a CH_4 flux from the frozen lake to the atmosphere, following the partial pressure gradient. However, this flux is suspended for impermeable ice. The permeability of the ice is mainly depended on the salinity and temperature of the ice (Lovely et al., 2015; Thomas, 2012). Both water bodies, lagoon and bay, are characterized by brackish water. Thus the salinity in both lakes is comparable and lower than 2 PSU. Therefore, the permeability varies mainly by differences in temperature. Ice with temperatures higher than –1.5 C is permeable, while ice with temperatures lower than –1.5°C is impermeable and gas migration is inhibited (Gosink et al., 1976). As described in the previous section, the freezing processes in Tiksi Bay and Polar Fox Lagoon differ from each other. The lagoon is a semi-closed system. The upper ice was influenced by water from the bay while the lower portion of the ice was formed during freezing in a closed system. By comparison, Tiksi bay is an open system and the ice was consequently characterised by an open freezing process, the lower ice portion was additionally affected by water mixing.

A semi-closed system – Polar Fox Lagoon

As discussed in the previous chapter, the water composition of Polar Fox showed clearly different freezing processes between the upper portion of the ice (0 - 60 cm) and the lower portion of the ice (> 60 cm). Polar Fox Lagoon was transformed into a closed system during freezing (see previous section). Remarkable is, that the CH_4 concentration changed contemporaneously. In the depth between 0 - 60 cm, i.e. formed in a still open system but tending towards a closed system, concentration was highest at the top of the ice and increased between 30 and 60 cm (**Figure 10**, chapter 4). Compared to this upper 60 cm section, constantly lower concentrations occurred between 60 - 140 cm in the ice, i.e. in a closed freezing system. The strong increase in CH_4 concentration in ice, at depths > 140 cm (**Figure 10**, chapter 4) is not accompanied by a change in the freezing processes. In addition to the increased CH_4 concentration, the temperatures increased towards the bottom of the ice (**Figure 5**, chapter 4). The increase in temperature clearly points to a higher permeability in this portion. Temperatures above –1.5°C occurred only in the lowest 24 cm of the ice (**Table 4**, Appendix) and give evidence that CH_4 is transported from the water into this portion of the ice. This is corroborated by the concentration maxima (about 540 nM) at the bottom ice. Enhanced CH_4 concentration at

the ice-water interface during winter is also shown by (Boereboom et al., 2012). During winter, much of the ebullition bubbles were trapped in and beneath the ice, as dissolved gases were stored under the ice (Walter Anthony et al., 2010).

An open system – Tiksi Bay

Tiksi Bay is connected to the Laptev Sea and therefore classified as an open water body with water depths about 4 - 10 m (Lantuit et al., 2011). In comparison to the semi-closed Polar Fox Lagoon, ice from the Tiksi Bay reflects freezing in an open system. Using the $\delta^{18}O/\delta D$ signatures and EC, the ice cores from Tiksi Bay can be distinguished in an upper part ($\leq$ 80 - 90 cm) and lower part (> 80 - 90 cm). The upper part clearly reflects freezing from brackish bay water, whereas the lower part reveals a higher amount of Lena river water to the frozen bay water (see previous chapter).

In the same way, methane concentrations were homogenously slightly supersaturated in the upper ice. In the lower ice, methane concentrations decreased slightly compared to the upper ice (**Figure 11**, chapter 4) and were partly lower than the saturation concentration of ~5 nM. An influence of methane uptake from the water into the ice cannot be precisely determined, as there were no methane data for the last 30 cm of the ice. However, temperatures warmer than –1.5°C for the last 40 cm of the ice occurred for core 29 (**Table 4**, appendix) indicating permeability for the whole last part of the ice here. Therefore, these concentrations might be still influenced by methane diffusion from the water into the ice. The methane concentrations slightly decreased further in the last, permeable two measured depths of core 29 (**Figure 11**, chapter 4). This suggested similar or even lower methane concentrations in the water under the ice as in the ice cores. Hence, accumulation of methane in the water under the ice was probably not as important in Tiksi Bay as it was in Polar Fox Lagoon.

To summarize, in both systems freezing processes and methane concentrations are correlated. The simultaneous change of freezing and concentration of methane is more evident in Polar Fox Lagoon than in Tiksi Bay. A considerable aspect is that both, the freezing processes as well as the solubility of methane, is depended on salinity and temperature. Also the permeability of the ice plays an important role for the methane dynamics in the ice. Furthermore, the methane concentration was affected by methane oxidation in the ice after freezing. This process will be discussed in detail in the following section.

5.3 Bacterial methane oxidation in bottom ice

The process of oxidation is shown in the depletion of ^{12}C, due to the favoured bacterial consumption of ^{12}C. This leads to an increase in the carbon isotopic signal of CH_4 ($\delta^{13}C_{CH4}$) (Whiticar, 1999). For both water bodies, a Rayleigh distillation model of the type discussed by Coleman et al. (1981) and used by Damm et al. (2015) and Damm et al. (2005) was calculated:

$$\delta_{13}C_{CH4} = 1000 * \left(\frac{1}{\alpha} - 1\right) * \ln f + (\delta_{13}C_{CH4})_0 \quad (6)$$

where α is the isotope fractionation factor, *f* is the fraction of the CH_4 remaining and $(\delta^{13}C_{CH4})_0$ is the initial isotopic composition.For the Rayleigh model it is assumed that bacterial oxidation is the only sink of CH_4, no further inputs and mixing occur, which would affect the isotopic composition of CH_4 (Mook, 1994). For Polar Fox Lagoon and Tiksi Bay α was determined as 1.004, whereas in marine environments α is 1.008 (Damm et al., 2005; Mau et al., 2013). This means that CH_4 consumption in Polar Fox Lagoon and Tiksi Bay occurred with a slightly lower increase of $\delta^{13}C_{CH4}$ than in marine environments.

Oxidation in the semi-closed system

Figure 14 shows the CH_4 concentrations versus the $\delta^{13}C_{CH4}$ values and the Rayleigh curves (lines) for the top and bottom ice of Polar Fox Lagoon. The Rayleigh curves show the same trend as the values of the ice strongly suggesting an oxidation process at the bottom of the ice. An oxidation signal is also clearly shown in the lower portion of the ice, where the $\delta^{13}C_{CH4}$ of CH_4 reached a maximum of approximately –32 ‰. In the lower portion of the ice (60 – 140 cm), low concentrations of ~ 3 nM indicate threshold values (**Figure 10**, chapter 4). This threshold values are the CH_4 concentration remaining when oxidation ceases. Oxidation for concentrations < 10 nM is slow (Cowen et al,, 2002; Valentine et al., 2001) and threshold values in nature are less than 10 nM (Hanson & Hanson, 1996) while (Valentine et al., 2001) investigated thresholds higher than 10 nM CH_4 in pure cultures of methanotrophs.

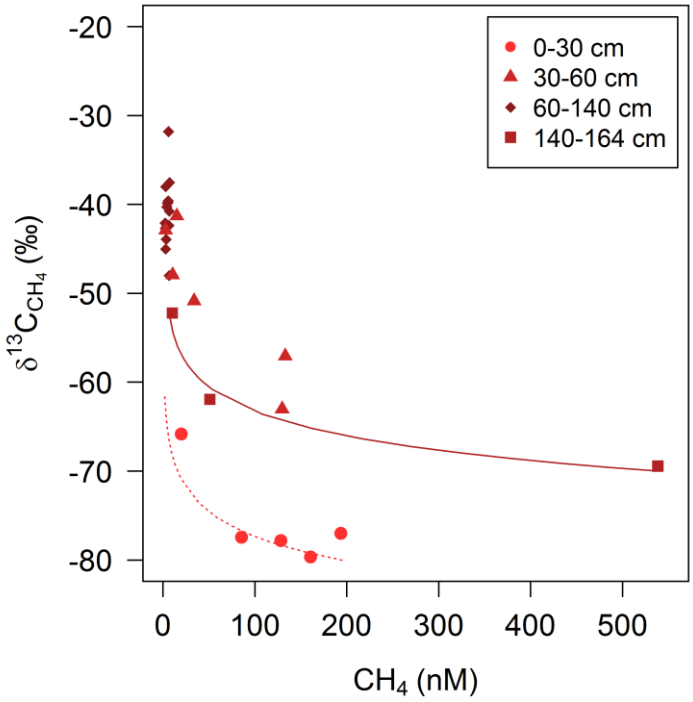

Figure 14: Methane oxidation in the Polar Fox Lagoon ice cores calculated by a Rayleigh fractionation model (see text). The curves show the prospective $\delta^{13}C_{CH4}$ signatures modified by oxidation. The methane consumed by oxidation was calculated by the initial, highest concentration detected at the bottom of the ice core (450 nM, dark red, solid line) and at the top (195 nM , red, dotted line). The initial isotopic signature was –80 ‰ (red, dotted line) and –70 ‰ (dark red, solid line). For both fraction curves $\alpha = 1.004$ fit best, i.e. the oxidation efficiency was comparable.

In contrast, ice between 0-60 cm had values between ~ 11 nM (50 - 60 cm) and about 194 nM (20 - 30 cm) (**Table 4**, Appendix). This shows that totally efficient oxidation started from the ice depth of 60 cm, where the freezing process of Polar Fox Lagoon changed. The Polar Fox Lagoon ice clearly points to an increased uptake of CH_4, likely from gas bubbles in the bottom ice. The bottom ice offers a protected environment and good conditions for bacteria. Temperatures increased to almost –0.5°C at the bottom of the ice, the ice was in contact with the water and permeable, permitting migration of gases and nutrients. For sea ice, most bacteria are located in the lowest centimetres of the ice (Krembs & Engel, 2001). As the ice grows, its growth rate decreases (Anderson, 1961). With decreasing ice growth rate, there is more time and space for CH_4 oxidizing bacteria to metabolize, as subsequent ice forms more slowly. Hence, the progress of freezing facilitates the oxidation process in the ice. The process of CH_4 uptake from the water into the bottom of the ice and its oxidation there may continue over the winter until the ice break-up, but this process is linked to the dissolved concentrations of oxygen. During winter, in shallow lakes with a small water volume and a small oxygen storage, CH_4 accumulation in the water is likely due to the lack of oxidation (Juutinen et al., 2009). DOC may also be a potential source for CH_4 production in lake waters (Striegl & Michmerhuizen,

1998) and could contribute to CH_4 accumulation. DOC was available at Polar Fox Lagoon. DOC concentrations increased with depth in the ice, with values up to 3.55 mg L^{-1}. In the upper ice, DOC concentrations were highly variable and ranged from 0.66 mg L^{-1} to 3.31 mg L^{-1} (0 - 60 cm) (**Figure 5**, chapter 4). CH_4 concentrations were variable in this portion as well and indicated a similar pattern as DOC concentrations (**Figure 5, Figure 10**, chapter 4). For Tiksi Bay DOC concentrations ranged from 1.00 mg L^{-1} to 2.93 mg L^{-1} (**Table 2**, chapter 4) and showed a similar trend as CH_4 concentrations in the ice (**Figure 8, Figure 11**, chapter 4), which suggest that the mixing of water (see 5.1, Tiksi Bay), may have had an influence on both DOC and CH_4 concentrations. However, DOC and CH_4 concentrations do not indicate a significant correlation for the different portions of the ice at Polar Fox Lagoon or Tiksi Bay. The transformation from DOC to CH_4 is therefore neither confirmed nor falsified by the data of this study and requires further investigation.

Oxidation in the open system

In contrast to the closed system (Polar Fox), the open system (Tiksi Bay) is more dynamic, as it is influenced by mixing and dilution of different waters and potentially oxidation therein. A large amount of CH_4 can be oxidized at the sediment surface or in the water column (Bussmann et al., 2017; Juutinen et al., 2009). Potential environments for CH_4 oxidation are the sediments, the water column and the ice. The study of Overduin et al. (2015a) examined CH_4 oxidation in the submarine permafrost in the East Sibirian Arctic shelf region (Buor Khaya Bay, central Laptev Sea) and other studies (e.g. Damm et al., 2007; Mau et al., 2013; Valentine et al., 2001) investigated CH_4 oxidation in coastal or shelf waters. In addition, the data of Polar Fox Lagoon demonstrated the bottom of the ice as a further potential environment for CH_4 oxidation. However, in Tiksi Bay the concentrations < 10 nM were in the range of CH_4 surface water concentrations (2.1 nM to 28.2 nM) from the East Siberian Arctic shelf (Shakhova & Semiletov, 2007) and for Buor-Khaya Bay, with medium concentrations of 26 - 33 nM (Bussmann, 2013). The water concentrations were lower than sediment concentrations, with a mean CH_4 concentration in overlying unfrozen sediment layers of 7.1 ± 24.9 µM and 380.6 ± 354.9 µM in the underlying frozen sediments with simultaneously occurred mean $\delta^{13}C_{CH4}$ values of -36.9 ± 9.3 ‰ and -62.4 ± 6.5 ‰, respectively (Overduin et al., 2015a). These results show CH_4 oxidation in the sediments as well as in the water column. Moreover, CH_4 values in the ice were comparable to but slightly higher than values in other surface shelf waters (Damm et al., 2005), where the mean concentration of the surface- and subsurface waters was 3.3 nM and the $\delta^{13}C_{CH4}$ value –44.5 ‰. Also the permeable ice in core 29 of Tiksi Bay indicated no diffusion from the water into the ice. These findings suggest low CH_4

concentration in the water under the ice, either due to low original CH_4 concentrations and/or to oxidation in the water column.

Figure 15 shows the Rayleigh distillation model for Tiksi Bay. The CH_4 concentrations and $\delta^{13}C_{CH4}$ values varied just slightly and the lower ice section (≥ 80 - 90 cm) was slightly more depleted in ^{12}C. Furthermore, the values scattered around the calculated oxidation curve. This indicated that other processes, such as dilution or mixing, affected the isotopic composition. This influence was stronger in the lower ice section than in the upper ice section. Lower concentrations with the same $\delta^{13}C_{CH4}$ value indicate dilution (Damm et al., 2005). The dilution effect was more recognizable with increased distance from the shore, and increased water depth (core 30: 2.84 m, core 29: 3.87 m, core 28: 3.3 m, core 27: 4.21 m). The CH_4 concentrations were generally highest in core 30, which was closest to the shore (mean: 7.23 nM) and lowest in core 27, furthest from shore (mean: 5.11 nM). The $\delta^{13}C_{CH4}$ values were similar for all cores, with mean values of –45.6 ‰ (core 30) and –46.8 ‰ (core 27) (**Table 3**, chapter 4). In general, the results suggest a homogeneous oxidation process over winter, with a slight change to lower concentrations when mixing with fresher water occurred and a distinct but slight increasing dilution signal with distance from shore.

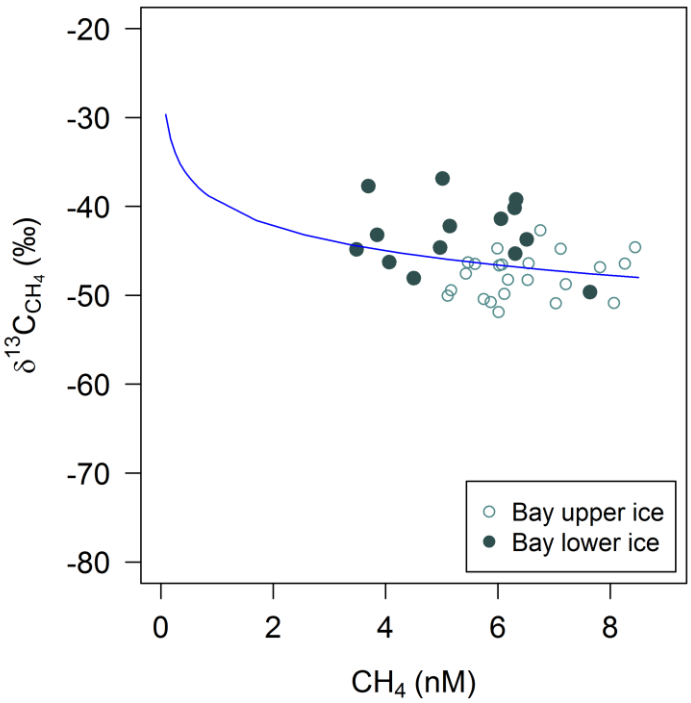

Figure 15: Methane oxidation in the Tiksi Bay ice cores calculated by a Rayleigh fractionation model (see text). The curve shows the prospective $\delta^{13}C_{CH4}$ signatures modified by oxidation. The methane consumed by oxidation was calculated by the initial, highest concentration (8.5 nM). The initial isotopic signature was –48 ‰. Also for this fraction curve $\alpha = 1.004$ fits best, like for Polar Fox.

Comparison of the two systems

In contrast to Polar Fox Lagoon, CH_4 concentrations of Tiksi Bay varied only over a small range. Therefore, the process of bacterial CH_4 oxidation could only be clearly identified in the ice of Polar Fox Lagoon. In the closed and shallow lagoon, CH_4 that had accumulated under the ice presumably enhanced the potential for CH_4 oxidation. In contrast, CH_4 concentrations in the ice of the open bay were influenced by mixing and dilution before freezing. Oxidation likely occurred in the sediments and the water column, decreasing the potential for CH_4 oxidation to occur.

Error analyses and limitations of the research

A number of limitations may have influenced the results of this study. One issue was the time intervening between the field sampling and analyses. It took about half a year for sample transport from the field site to the laboratory, i.e. between coring and analysis. Another point is the representation of the data. Repeated measurements from multiple cores from one location or even comparing measurements from more samples for one parameter from one core and at different locations in the lagoon would improve the database and allow a reliable statistical evaluation.

In total, these sources of error suggest improvements to ice core handling and sampling for future studies. In particular, multiple cores from some sites should be collected to control for spatial variability and allow for sampling after different storage times. If possible, the time period between coring and sectioning should be reduced to control for post-sampling changes to measured parameters.

If changes took place, they probably did not affect the results sufficiently to change our interpretation, since the concentrations and stable isotope signatures of the cores, taken in the context of the freezing processes evident from the stable isotopes of water and hydrochemistry, clearly indicate the presence of significant amounts of CH_4 and of its oxidation. The changes in the data are reasonable and do not suggest that the time period between the sampling and analyses or the handling influenced the results significantly.

6 Conclusions

In this thesis, CH_4 concentrations were studied in Polar Fox Lagoon, a coastal lagoon connected to the sea during summer, and in offshore waters of Tiksi Bay, Siberia. Polar Fox Lagoon is a semi-closed system, with seawater influx during the open water season but isolated and with significant water volume reduction during the winter. On the other hand, Tiksi Bay is open to the central Laptev Sea throughout the winter and shares its stratified water column.

Differences between the two systems influenced the CH_4 concentrations observed in the ice. In Polar Fox Lagoon, CH_4 concentrations in the ice varied greatly, whereas Tiksi Bay showed generally low CH_4 concentrations and reflected water background CH_4 concentrations and $\delta^{13}C_{CH4}$ values.

Assuming consistently high CH_4 concentrations in the lagoon water over the winter, CH_4 concentration and the $\delta^{13}C_{CH4}$ values in the ice cover of Polar Fox Lagoon showed the effect of CH_4 oxidation. Bacterial oxidation thus reduces the CH_4 concentrations during the winter at Polar Fox Lagoon. The oxidation depleted dissolved CH_4 at the ice-water interface, where ice temperatures are warmest, the water-ice environment provides a habitat for organisms and gas migration into the ice and the water column provides a source of dissolved CH_4. Continuing ice growth during freezing separates older ice from interaction with the water column. When the older ice becomes impermeable, CH_4 is frozen into the ice, archiving an oxidation signal, even if no further oxidation occurs.

These results permit calculation of CH_4 production (methanogenesis) and CH_4 consumption (oxidation) budgets, which could help to quantify the efficacy of CH_4 oxidation during winter for Polar Fox Lagoon and coastal lagoons in general.

Oxidation may limits the CH_4 concentrations emitting from the lakes to the atmosphere after the ice break-up in spring. Arctic warming will continue to shorten ice cover duration. Since high-latitude lakes emit large amounts of CH_4 during ice melt, an understanding of CH_4 pathways in and below ice in Arctic lakes, lagoons and coastal waters is important to understand their role in the global warming cycle and for better simulation of future climate scenarios.

As the sediment is a known environment for CH_4 production and DOC could be a source for CH_4 production in the water or the ice, sediment pore water $\delta^{13}C_{CH4}$ values, CH_4 and DOC concentrations from Polar Fox Lagoon and Tiksi Bay should be considered to understand CH_4 pathways in such water bodies. The determination of the sources for CH_4 production are particularly interesting for Polar Fox Lagoon, where the accumulation of CH_4 under the ice was evident. Furthermore, the comparison between brackish and freshwater water bodies in terms

of CH_4 oxidation may yield insights into the circumstances under which CH_4 oxidation occurs in thermokarst lakes and Arctic lagoons. As CO_2 is an important greenhouse gas and the product of CH_4 oxidation, future studies need to include both greenhouse gases in their analyses.

7 Danksagung

Ich bedanke mich bei allen, die mich bei meiner Masterarbeit unterstützt haben.

Mein besonderer Dank gilt meinen Betreuern, die mir das Anfertigen dieser Arbeit ermöglicht haben. Guido danke ich für die Übernahme des Erstgutachters, wodurch es mir möglich war diese Arbeit in diesem Rahmen anzufertigen.

Ellen und Paul, euch danke ich besonders für die ausdauernde Betreuung, viele bereichernde Kommentare, Anmerkungen, Diskussionen und Ratschläge. Die Zeit meiner Masterarbeit war für mich eine sehr lehrreiche und spannende Zeit.

Ellen, bei dir bedanke ich mich darüber hinaus für deinen unermüdlichen Einsatz ein passendes Masterarbeitsthema mit mir zu finden.

Hanno, Mike und Ingeborg möchte ich für hilfreiche Anregungen und Diskussionen danken. Bei Ingeborg und Yoga bedanke ich mich außerdem für den Austausch und die Gastfreundschaft auf Helgoland.

Ebenfalls bedanken möchte ich mich bei allen, die mich im Labor in Potsdam, Bremerhaven und Bremen unterstützt haben, insbesondere bei Antje, für die tolle Einführung und Zusammenarbeit im Labor und ein stets offenes Ohr. Und bei allen weiteren, die die Daten erhoben und mir einen so spannenden Datensatz zur Verfügung gestellt haben.

Bei meinen Freunden bedanke ich mich für die hilfreichen Diskussionen und motivierenden Gespräche. Insbesondere Alex und Sophia für das Korrekturlesen und Hilfe mit R, sowie Thomas für seine Ruhe und Gelassenheit, die mich immer wieder darin bestärkt haben weiterzumachen

Meinen Eltern möchte ich danken, dass sie mich während meines gesamten Studiums unterstützt haben und mich immer darin bestärkt haben meinen Interessen nachzugehen.

8 References

Adams, W. P., & Lasenby, D. C. (1985). The roles of snow, lake ice and lake water in the distribution of major ions in the ice cover of a lake. *Annals of Glaciology*, *7*, 202–207.

Alekseevskii, N. I., Aibulatov, D. N., Kuksina, L. V, & Chetverova, A. A. (2014). The structure of streams in the Lena delta and its influence on streamflow transformation processes. *Geography and Natural Resources*, *35*(1), 63–70. https://doi.org/10.1134/S1875372814010090

Anderson, D. L. (1961). Growth rate of sea ice. *Journal of Glaciology*, *3*(30), 1170–1172.

Antonova, S., Duguay, C. R., Kääb, A., Heim, B., Langer, M., Westermann, S., & Boike, J. (2016). Monitoring bedfast ice and ice phenology in lakes of the Lena river delta using TerraSAR-X backscatter and coherence time series. *Remote Sensing*, *8*(11). https://doi.org/10.3390/rs8110903

Arnason, B. (1969). Equilibrium constant for the fractionation of deuterium between ice and water. *Journal of Physical Chemistry*, *73*(10), 3491-3494

Bastviken, D., Cole, J. J., Pace, M. L., & Van de-Bogert, M. C. (2008). Fates of methane from different lake habitats: Connecting whole-lake budgets and CH4emissions. *Journal of Geophysical Research: Biogeosciences*, *113*(2), 1–13. https://doi.org/10.1029/2007JG000608

Bastviken, D., Cole, J., Pace, M., & Tranvik, L. (2004). Methane emissions from lakes: Dependence of lake characteristics, two regional assessments, and a global estimate. *Global Biogeochemical Cycles*, *18*(4), GB4009. https://doi.org/10.1029/2004GB002238

Bastviken, D., Ejlertsson, J., & Tranvik, L. (2002). Measurement of Methane Oxidation in Lakes: A Comparison of Methods. *Environ. Sci. Technol.*, *36*(15), 3354–3361. https://doi.org/DOI: 10.1021/es010311p

Boereboom, T., Depoorter, M., Coppens, S., & Tison, J. L. (2012). Gas properties of winter lake ice in Northern Sweden: Implication for carbon gas release. *Biogeosciences*, *9*(2), 827–838. https://doi.org/10.5194/bg-9-827-2012

Boike, J., El-Hajj, H., Morgenstern, A., Overduin, P.P., & Strauss, J. (eds). Russian-German Cooperation: Expeditions to Siberia in 2017, Berichte zur Polar- und Meeresforschung, Reports on polar and marine research, Bremerhaven, Alfred Wegener Institute for Polar and Marine Research, in preparation.

Bussmann, I. (2013). Distribution of methane in the Lena Delta and Buor-Khaya Bay, Russia. *Biogeosciences*, *10*(7), 4641–4652. https://doi.org/10.5194/bg-10-4641-2013

Bussmann, I., Hackbusch, S., Schaal, P., & Wichels, A. (2017). Methane distribution and oxidation around the Lena Delta in summer 2013. *Biogeosciences*, *14*(21), 4985–5002. https://doi.org/10.5194/bg-14-4985-2017

Cole, J. J., Prairie, Y. T., Caraco, N. F., McDowell, W. H., Tranvik, L. J., Striegl, R. G., … Melack, J. (2007). Plumbing the Global Carbon Cycle: Integrating Inland Waters into the Terrestrial Carbon Budget. *Ecosystems*, *10*(1), 172–185. https://doi.org/10.1007/s10021-006-9013-8

Coleman, D. D., Risatti, J. B., & Schoell, M. (1981). Fractionation of carbon and hydrogen isotopes by methane oxidizing bacteria. *Geochimica Cosmochimica Acta*, *45*, 1033–1037.

Cottier, F., Eicken, H., & Wadhams, P. (1999). Linkages between salinity and brine channel distribution in young sea ice. *Journal of Geophysical Research*, *104*(C7), 15,859-15,871.

Cowen, J. P., Wen, X., & Popp, B. N. (2002). Methane in aging hydrothermal plumes. *Geochimica et Cosmochimica Acta*, *66*(20), 3563–3571. https://doi.org/10.1016/S0016-7037(02)00975-4

Craig, H. (1961). Isotopic variations in meteoric waters. *Science*, *133*(3465), 1702–1703.

Damm, E., Mackensen, A., Budéus, G., Faber, E., & Hanfland, C. (2005). Pathways of methane in seawater: Plume spreading in an Arctic shelf environment (SW-Spitsbergen). *Continental Shelf Research*, *25*(12–13), 1453–1472. https://doi.org/10.1016/j.csr.2005.03.003

Damm, E., Rudels, B., Schauer, U., Mau, S., & Dieckmann, G. (2015). Methane excess in Arctic surface water-triggered by sea ice formation and melting. *Scientific Reports*, *5*, 1–9. https://doi.org/10.1038/srep16179

Damm, E., Schauer, U., Rudels, B., & Haas, C. (2007). Excess of bottom-released methane in an Arctic shelf sea polynya in winter. *Continental Shelf Research*, *27*(12), 1692–1701. https://doi.org/10.1016/j.csr.2007.02.003

Dansgaard, W. (1964). Stable isotopes in precipitation. *Tellus*, *16*(4), 436–468. https://doi.org/10.3402/tellusa.v16i4.8993

Denfeld, B. A., Baulch, H. M., del Giorgio, P. A., Hampton, S. E., & Karlsson, J. (2018). A synthesis of carbon dioxide and methane dynamics during the ice-covered period of northern lakes. *Limnology and Oceanography Letters*, *3*(3), 117–131. https://doi.org/10.1002/lol2.10079

Fedorova, I., Chetverova, A., Bolshiyanov, D., Makarov, A., Boike, J., Heim, B., … Sidorina, I. (2015). Lena Delta hydrology and geochemistry: Long-term hydrological data and recent field observations. *Biogeosciences*, *12*(2), 345–363. https://doi.org/10.5194/bg-12-345-2015

Fung, I., John, J., Lerner, J., Matthews, E., Prather, M., Steele, L. P., & Fraser, P. J. (1991). Three-dimensional model synthesis of the global methane cycle. *Journal of Geophysical Research*, *96*(D7), 13033. https://doi.org/10.1029/91JD01247

Gibson, J. J., & Prowse, T. D. (1999). Isotopic characteristics of ice cover in a large northern river basin. *Hydrological Processes*, *13*(16 SPEC. ISS.), 2537–2548. https://doi.org/10.1002/(SICI)1099-1085(199911)13:16<2537::AID-HYP940>3.0.CO;2-A

Gibson, J. J., & Prowse, T. D. (2002). Stable isotopes in river ice: Identifying primary over-winter streamflow signals and their hydrological significance. *Hydrological Processes*, *16*(4), 873–890. https://doi.org/10.1002/hyp.366

Gosink, T.A., J.G. Pearson, & J.J. Kelly. 1976. Gas movement through sea-ice. *Nature 263*, 41-42. http://dx.doi.org/10.1038/263041a0.

Grosse, G., Schirrmeister, L., Kunitsky, V. V, & Hubberten, H.-W. (2005). The Use of CORONA Images in Remote Sensing of Periglacial Geomorphology: An Illustration from the NE Siberian Coast. *Permafrost and Periglacial Processes*, *16*, 163–172. https://doi.org/10.1002/ppp.509

Grosse, G., Schirrmeister, L., Siegert, C., Kunitsky, V. V, Slagoda, E. A., Andreev, A. A., & Dereviagyn, A. Y. (2006). Geological and geomorphological evolution of a sedimentary periglacial landscape in Northeast Siberia during the Late Quaternary. *Geomorphology*. https://doi.org/10.1016/j.geomorph.2006.08.005

Günther, F. G., Overduin, P. P., Sandakov, A. V, Grosse, G., & Grigoriev, M. N. (2013). Short- and long-term thermo-erosion of ice-rich permafrost coasts in the Laptev Sea region. *Biogeosciences*, *10*, 4297–4318. https://doi.org/10.5194/bg-10-4297-2013

Günther, F., Overduin, P. P., Yakshina, I. A., Opel, T., Baranskaya, A. V., & Grigoriev, M. N. (2015). Observing Muostakh disappear: Permafrost thaw subsidence and erosion of a ground-ice-rich Island in response to arctic summer warming and sea ice reduction. *Cryosphere*, *9*(1), 151–178. https://doi.org/10.5194/tc-9-151-2015

Hanson, R. S., & Hanson, T. E. (1996). Methanotrophic Bacteria. *Microbiological Reviews*, *60*(2), 439–471.

IPCC, 2013: Climate Change 2013: The Physical Science Basis. Contribution of Working Group I to the Fifth Assessment Report of the Intergovern-mental Panel on Climate Change [Stocker, T.F., D. Qin, G.-K. Plattner, M. Tignor, S.K. Allen, J. Boschung, A. Nauels, Y. Xia, V. Bex and P.M. Midgley (eds.)]. *Cambridge University Press*, United Kingdom and New York, NY, USA, 1535pp.

Janout, M., Hölemann, J., Juhls, B., Krumpen, T., Rabe, B., Bauch, D., … Timokhov, L. (2016). Episodic warming of near-bottom waters under the Arctic sea ice on the central Laptev Sea shelf. *Geophysical Research Letters*. https://doi.org/10.1002/2015GL066565

Juutinen, S., Rantakari, M., Kortelainen, P., Huttunen, J. T., Larmola, T., Alm, J., … Martikainen, P. J. (2009). Methane dynamics in different boreal lake types. *Biogeosciences*, *6*(2), 209–223. https://doi.org/10.5194/bg-6-209-2009

Karlsson, J., Giesler, R., Persson, J., & Lundin, E. (2013). High emission of carbon dioxide and methane during ice thaw in high latitude lakes. *Geophysical Research Letters*, *40*(6), 1123–1127. https://doi.org/10.1002/grl.50152

Kelly, C. A., & Chynoweth, D. P. (1981). The contributions of temperature and of the input of organic matter in controlling rates of sediment methanogenesis1. *Limnol. Oceanogr*, *26*(5), 891–897.

Koven, C. D., Ringeval, B., Friedlingstein, P., Ciais, P., Cadule, P., Khvorostyanov, D., … Tarnocai, C. (2011). Permafrost carbon-climate feedbacks accelerate global warming. *Proceedings of the National Academy of Sciences*, *108*(36), 14769–14774. https://doi.org/10.1073/pnas.1103910108

Krembs, C., & Engel, A. (2001). Abundance and variability of microorganisms and transparent exopolymer particles across the ice-water interface of melting first-year sea ice in the Laptev Sea (Arctic). *Marine Biology*, *138*(1), 173–185. https://doi.org/10.1007/s002270000396

Kuhn, W., & Thürkauf, M. (1958). Isotopentrennung beim Gefrieren von Wasser und Diffusionskonstanten von D und 18O im Eis. Mit Diskussion der Möglichkeit einer Multiplikation der beim Gefrieren auftretenden Isotopentrennung in einer Haarnadelgegenstromvorrichtung. *Helvetica Chimica Acta*, *41*(4), 938-971

Lacelle, D. (2011). On the d18O, dD and D-excess Relations in Meteoric Precipitation and During Equilibrium Freezing: Theoretical Approach and Field Examples. *Permafrost and Periglacial Processes*, *22*, 13–25. https://doi.org/10.1002/ppp.712

Langer, M., Westermann, S., Anthony, K. W., Wischnewski, K., & Boike, J. (2015). Frozen ponds: production and storage of methane during the Arctic winter in a lowland tundra landscape in northern Siberia, Lena River delta. *Biogeosciences*, *12*, 977–990. https://doi.org/10.5194/bg-12-977-2015

Lantuit, H., Atkinson, D., Overduin, P. P., Grigoriev, M., Rachold, V., Grosse, G., & Hubberten, H.-W. (2011). Coastal erosion dynamics on the permafrost-dominated Bykovsky Peninsula, north Siberia, 1951-2006. *Polar Research*, *30*(1), 7341. https://doi.org/10.3402/polar.v30i0.7341

Lehmann, M., & Siegenthaler, U. (1991). Equilibriunl oxygen-and hydrogen-isotope fractionation between ice and water. *Journal of Glaciology*, *37*(125), 23–26. https://doi.org/10.3198/1991JoG37-125-23-26

Lidstrom, M. E., & Somers, L. (1984). Seasonal study of methane oxidation in Lake Washington. *Applied and Environmental Microbiology*, *47*(6), 1255–1260.

Lindgren, P. R., Grosse, G., Anthony, K. M. W., & Meyer, F. J. (2016). Detection and

spatiotemporal analysis of methane ebullition on thermokarst lake ice using high-resolution optical aerial imagery. *Biogeosciences*, *13*, 27–44. https://doi.org/10.5194/bg-13-27-2016

Lovely, A., Loose, B., Schlosser, P., McGillis, W., Zappa, C., Perovich, D., … Friedrich, R. (2015). The Gas Transfer through Polar Sea ice experiment: Insights into the rates and pathways that determine geochemical fluxes. *Journal of Geophysical Research: Oceans*, *120*(12), 8177–8194. https://doi.org/10.1002/2014JC010607

Magritsky, V. V, Aibulatov, D. N., & Gorelkin, A. V. (2018). Regularities in the Space and Time Flow Variations in the Near-Mouth Reach and Delta of the Lena R. *Water Resources*, *45*(1), 15–29. https://doi.org/10.1134/S009780781801013X

Martinez-Cruz, K., Sepulveda-Jauregui, A., Walter Anthony, K., & Thalasso, F. (2015). Geographic and seasonal variation of dissolved methane and aerobic methane oxidation in Alaskan lakes. *Biogeosciences*, *12*(15), 4595–4606. https://doi.org/10.5194/bg-12-4595-2015

Massom, R. A., & Stammerjohn, S. E. (2010). Antarctic sea ice change and variability - Physical and ecological implications. *Polar Science*, *4*(2), 149–186. https://doi.org/10.1016/j.polar.2010.05.001

Mau, S., Blees, J., Helmke, E., Niemann, H., & Damm, E. (2013). Vertical distribution of methane oxidation and methanotrophic response to elevated methane concentrations in stratified waters of the Arctic fjord Storfjorden (Svalbard, Norway). *Biogeosciences*, *10*(10), 6267–6268. https://doi.org/10.5194/bg-10-6267-2013

McDougall, T.J. and P.M. Barker, (2011). Getting started with TOES-10 and the Gibbs Seawater (GSW) Oceanographic Toolbox, *SCOR/IAPSO WG127*, ISBN 978-0-646-55621-5, 28pp.

Meyer, H., Dereviagin, A. Y., Siegert, C., & Hubberten, H.-W. (2002). Paleoclimate studies on Bykovsky Peninsula, North Siberia-hydrogen and oxygen isotopes in ground ice. *Polarforschung*, *70*, 37–51.

Michmerhuizen, C. M., Striegl, R. G., & McDonald, M. E. (1996). Potential methane emission from north-temperate lakes following ice melt. *Limnology and Oceanography*, *41*(5), 985–991. https://doi.org/10.4319/lo.1996.41.5.0985

Mook, W. G. (1994). Principles of isotope hydrology. Introductory course on Isotope Hydrology. Dep. Hydrogeol. Geogr. Hydrol., *VU Amsterdam, Amsterdam.*

Morimoto, M., Kawanobe, K., Abe, O., Kawai, T., Kawamura, T., & Shirasawa, K. (2010). Under-ice salinity and stable isotope distribution of Saroma-ko Lagoon, Hokkaido, northern Japan. *Hydrological Processes*, *24*(7), 904–916. https://doi.org/10.1002/hyp.7532

NOAA. (2018). Earth System Research Laboratory, Global Monitoring Division. URL:http://www. esrl.noaa.gov/gmd/dv/iadv/ (15.09.2018).

O'Neil, J. R. (1968). Hydrogen and oxygen isotope fractionation between ice and water. *Journal of Physical Chemistry, 72*(10), 3683-3684.

Overduin, P. , Blender, F. , Bolshiyanov, D. Y. , Grigoriev, M. N. , Morgenstern, A. and Meyer, H. (2017) Russian-German Cooperation: Expeditions to Siberia in 2016 ,Berichte zur Polar- und Meeresforschung, Reports on polar and marine research, Bremerhaven, Alfred Wegener Institute for Polar and Marine Research, 709 , 295 pp. doi:10.2312/BzPM_0709_2017

Overduin, P. P., Liebner, S., Knoblauch, C., Günther, F., Wetterich, S., Schirrmeister, L., … Grigoriev, M. N. (2015a). Methane oxidation following submarine permafrost degradation: Measurements from a central Laptev Sea shelf borehole. *Journal of*

Geophysical Research: Biogeosciences. https://doi.org/10.1002/2014JG002862

Overduin, P. P, Wetterich, S., Günther, F., Grigoriev, M. N., Grosse, G., Schirrmeister, L., … Makarov, A. (2015b). Coastal dynamics and submarine permafrost in shallow water of the central Laptev Sea, East Siberia. *Cryosphere Discussions*, *9*(4), 3741–3775. https://doi.org/10.5194/tcd-9-3741-2015

Parmentier, F. J. W., Christensen, T. R., Sørensen, L. L., Rysgaard, S., Mcguire, A. D., Miller, P. A., & Walker, D. A. (2013). The impact of lower sea-ice extent on Arctic greenhouse-gas exchange. *Nature Climate Change*, *3*, 195–202. https://doi.org/10.1038/nclimate1784

Phelps, A. R., Peterson, K. M., & Jeffries, M. O. (1998). Methane efflux from high-latitude lakes during spring ice melt. *Journal of Geophysical Research*, *103*(D22), 29029–29036. https://doi.org/10.1029/98JD00044

Powers, S. M., & Hampton, S. E. (2016). Winter Limnology as a New Frontier. *Limnology and Oceanography Bulletin*, *25*(4), 103–108. https://doi.org/10.1002/lob.10152

Ricão Canelhas, M., Denfeld, B. A., Weyhenmeyer, G. A., Bastviken, D., & Bertilsson, S. (2016). Methane oxidation at the water-ice interface of an ice-covered lake. *Limnology and Oceanography*, *61*, 78–90. https://doi.org/10.1002/lno.10288

Romanovskii, N. N., Hubberten, H.-W., Gavrilov, A. V, Tumskoy, V. E., Tipenko, G. S., Grigoriev, M. N., & Siegert, C. (2000). Thermokarst and land-ocean interactions, Laptev sea region, Russia. *Permafrost and Periglacial Processes*, *11*(2), 137–152. https://doi.org/10.1002/1099-1530(200004/06)11:2<137::AID-PPP345>3.0.CO;2-L

Rudd, J. W. M., & Hamilton, R. D. (1978). Methane cycling in a cutrophic shield lake and its effects on whole lake metabolism. *Limnol. Oceanogr*, *23*(2), 128.

Sasaki, M., Imura, S., Kudoh, S., Yamanouchi, T., Morimoto, S., & Hashida, G. (2009). Methane efflux from bubbles suspended in ice-covered lakes in Syowa Oasis, East Antarctica. *Journal of Geophysical Research Atmospheres*. https://doi.org/10.1029/2009JD011849

Schirrmeister, L., Grigoriev, M. N., Strauss, J., Grosse, G., Overduin, P. P., Kholodov, A., … Hubberten, H.-W. (2018). Sediment characteristics of a thermokarst lagoon in the northeastern Siberian Arctic (Ivashkina Lagoon, Bykovsky Peninsula). *Arktos*, *4*(1), 13. https://doi.org/10.1007/s41063-018-0049-8

Schirrmeister, L., Kunitsky, V., Grosse, G., Wetterich, S., Meyer, H., Schwamborn, G., … Siegert, C. (2010). Sedimentary characteristics and origin of the Late Pleistocene Ice Complex on north-east Siberian Arctic coastal lowlands and islands - A review. *Quaternary International*, *241*, 3–25. https://doi.org/10.1016/j.quaint.2010.04.004

Schirrmeister, L., Siegert, C., Kuznetsova, T., Kuzmina, S., Andreev, A., Kienast, F., … Bobrov', A. (2002). Palaeoenvironmental and Palaeoclimatic Records from Permafrost Deposits in the Arctic Region of Northern Siberia. *Quaternary International*, *89*(1), 97–118. https://doi.org/https://doi.org/10.1016/S1040-6182(01)00083-0

Schuur, E. A. G., Bockheim, J., Canadell, J. G., Euskirchen, E., Field, C. B., Goryachkin, S. V., … Zimov, S. A. (2008). Vulnerability of Permafrost Carbon to Climate Change: Implications for the Global Carbon Cycle. *BioScience*, *58*(8), 701–714. https://doi.org/10.1641/B580807

Schuur, E. A. G., McGuire, A. D., Schädel, C., Grosse, G., Harden, J. W., Hayes, D. J., … Vonk, J. E. (2015). Climate change and the permafrost carbon feedback. *Nature*, *520*(7546), 171–179. https://doi.org/10.1038/nature14338

SENTINEL Hub (2018) Laboratory for geographical information systems, Ltd. by SINGERGISE. URL: https://www.sentinel-hub.com/about (20.10.2018)

Shakhova, N., & Semiletov, I. (2007). Methane release and coastal environment in the East

Siberian Arctic shelf. *Journal of Marine Systems*, *66*(1–4), 227–243. https://doi.org/10.1016/j.jmarsys.2006.06.006

Souchez, R. A., & Jouzel, J. (1984). On the isotopic composition in δD and δ 18 O of water and ice during freezing. *Journal of Glaciology*, *30*(106), 369–372.

Striegl, R. G., & Michmerhuizen, C. M. (1998). Hydrologic influence on methane and carbon dioxide dynamics at two north-central Minnesota lakes. *Limnology and Oceanography*, *43*(7), 1519–1529. https://doi.org/10.4319/lo.1998.43.7.1519

Thomas, D. N. (2012). Sea ice. In E. M. Bell (Ed.), *Life at Extremes: Environments, Organisms, and Strategies for Survival* (pp. 62–80). Oxford, UK: CABI.

Valentine, D. L., Blanton, D. C., Reeburgh, W. S., & Kastner, M. (2001). Water column methane oxidation adjacent to an area of active hydrate dissociation, Eel River Basin. *Geochimica et Cosmochimica Acta*, *65*(16), 2633–2640. https://doi.org/10.1016/S0016-7037(01)00625-1

Walter Anthony, K. M., Vas, D. A., Brosius, L., Chapin, F. S., Zimov, S. A., & Zhuang, Q. (2010). Estimating methane emissions from northern lakes using ice- bubble surveys. *Limnology and Oceanography: Methods*, *8*, 592–609. https://doi.org/10:4319/lom.2010.8.592

Walter, K. M., Chanton, J. P., Chapin, F. S., Schuur, E. A. G., & Zimov, S. A. (2008). Methane production and bubble emissions from arctic lakes: Isotopic implications for source pathways and ages. *Journal of Geophysical Research: Biogeosciences*, *113*(3). https://doi.org/10.1029/2007JG000569

Walter, K. M., Edwards, M. E., Grosse, G., Zimov, S. A., & Chapin, F. S. (2007a). Thermokarst lakes as a source of atmospheric CH4 during the last deglaciation. *Science (New York, N.Y.)*, *318*(5850), 633–636. https://doi.org/10.1126/science.1142924

Walter, K. M., Smith, L. C., & Chapin, F. S. (2007b). Methane bubbling from northern lakes: present and future contributions to the global methane budget. *Philosophical Transactions of the Royal Society A: Mathematical, Physical and Engineering Sciences*, *365*(1856), 1657–1676. https://doi.org/10.1098/rsta.2007.2036

Walter, K. M., Zimov, S. A., Chanton, J. P., Verbyla, D., & Chapin, F. S. (2006). Methane bubbling from Siberian thaw lakes as a positive feedback to climate warming. *Nature*, *443*(7107), 71–75. https://doi.org/10.1038/nature05040

Whiticar, M. J. (1999). Carbon and hydrogen isotope systematics of bacterial formation and oxidation of methane. *Chemical Geology*, *161*(1), 291–314. https://doi.org/10.1016/S0009-2541(99)00092-3

Wiesenburg, D. A., & Guinasso, N. L. (1979). Equilibrium Solubilities of Methane, Carbon Monoxide, and Hydrogen in Water and Sea Water. *Journal of Chemical and Engineering Data*, *24*(4), 356–360. https://doi.org/10.1021/je60083a006

Wik, M., Crill, P. M., Bastviken, D., Danielsson, Å., & Norbäck, E. (2011). Bubbles trapped in arctic lake ice: Potential implications for methane emissions. *Journal of Geophysical Research: Biogeosciences*, *116*(3). https://doi.org/10.1029/2011JG001761

Wik, M., Varner, R. K., Anthony, K. W., MacIntyre, S., & Bastviken, D. (2016). Climate-sensitive northern lakes and ponds are critical components of methane release. *Nature Geoscience*, *9*(2), 99–105. https://doi.org/10.1038/ngeo2578

Wuebbles, D. J., & Hayhoe, K. (2002). Atmospheric methane and global change. *Earth-Science Reviews*, *57*(3–4), 177–210. https://doi.org/10.1016/S0012-8252(01)00062-9

Zeikus, J. G., & Winfrey, M. R. (1976). Temperature limitation of methanogenesis in aquatic sediments. *Applied and Environmental Microbiology*, *31*(1), 99–107.

Zhou, J., Tison, J.-L., Carnat, G., Geilfus, N.-X., & Delille, B. (2014). Physical controls on the

storage of methane in landfast sea ice. *The Cryosphere*, *8*, 1019–1029. https://doi.org/10.5194/tc-8-1019-2014

Zimov, S. A., Schuur, E. A. G., & Chapin, F. S. (2006). Permafrost and the Global Carbon Budget. *Science*, *312*(5780), 1612–1613.

Zimov, S. A., Voropaev, Y. V., Semiletov, I. P., Davidov, S. P., Prosiannikov, S. F., Chapin, F. S., … Tyler, S. (1997). North Siberian lakes: A methane source fueled by pleistocene carbon. *Science*, *277*(5327), 800–802. https://doi.org/10.1126/science.277.5327.800

9 Appendix

The following pages provide a table with the measured parameters for all cores with depths.

Table 4: Measured parameters listed for the four cores of Tiksi Bay (27, 28, 29 and 30) and the two course of Polar Fox Lagoon (31 and 32) with depth.

Core	Depth (cm)	$\delta^{18}O$ (‰)	δD (‰)	d exc (‰)	EC ($\mu S\ cm^{-1}$)	Salinity (PSU)	Average Temp. (°C)	DOC ($mg\ L^{-1}$)	Cl^- ($mg\ L^{-1}$)	SO_4^{2-} ($mg\ L^{-1}$)	CH_4 (nM)	$\delta^{13}C_{CH4}$ (‰)	pH
27	0-10	-15.3	-118.6	3.7	-	-	-7.8	-	-	-	-	-	-
27	10-20	-14.9	-115.0	4.4	1064	0.53	-7.3	1.56	-	-	5.2	-49.4	7.39
27	20-30	-14.9	-115.1	3.8	1291	0.64	-6.4	1.70	353	60.3	5.9	-50.8	7.38
27	30-40	-15.0	-115.5	4.5	1574	0.79	-5.7	2.07	429	74.4	5.7	-50.4	7.07
27	40-50	-14.7	-114.0	3.5	1724	0.87	-5.0	2.28	463	84.8	5.1	-50.0	6.67
27	50-60	-14.9	-114.6	4.3	1606	0.81	-4.6	2.05	436	74.9	6.0	-51.9	7.50
27	60-70	-15.2	-117.4	4.6	1549	0.78	-4.4	2.17	415	72.7	6.1	-49.8	6.79
27	70-80	-15.1	-116.0	4.7	-	-	-4.1	-	-	-	-	-	-
27	80-90	-15.8	-120.7	5.4	1460	0.73	-3.7	2.93	389	68.5	5.0	-36.9	6.77
27	90-100	-16.0	-122.8	5.4	645	0.31	-4.1	1.88	169	27.6	3.7	-37.7	6.84
27	100-110	-16.2	-124.3	5.2	340	0.16	-3.7	1.47	83.2	16.8	3.8	-43.2	6.43
27	110-120	-16.3	-125.0	5.2	604	0.29	-1.8	2.16	152	31.8	4.5	-48.1	6.82
27	125-135	-16.7	-128.1	5.3	-	-	-1.0	-	-	-	-	-	-
27	135-145	-16.5	-126.7	5.3	-	-	-0.7	-	-	-	-	-	-
27	145-155	-16.7	-128.7	5.1	-	-	-0.4	-	-	-	-	-	-
28	0-10	-15.7	-120.8	4.4	-	-	-6.8	-	-	-	-	-	-
28	10-19	-15.2	-116.8	4.6	1304	0.65	-6.5	1.71	350	61.3	6.1	-46.5	7.20

28	19-30	-15.1	-115.9	4.6	1674	0.84	-5.7	2.03	461	78.4	5.6	-46.4	7.14
28	30-42	-15.2	-116.7	5.1	2043	1.04	-5.1	2.35	505	97.9	5.5	-46.3	7.21
28	42-51	-15.2	-116.6	4.8	2065	1.05	-4.6	2.45	567	98.7	6.5	-48.3	7.33
28	51-60	-15.1	-116.0	5.0	1988	1.01	-4.2	2.32	548	95.9	6.2	-48.2	7.3
28	60-69	-15.7	-120.0	5.7	1752	0.88	-3.4	2.37	483	84.7	6.8	-42.7	7.29
28	70-80	-15.6	-120.0	5.2	-	-	-2.5	-	-	-	-	-	-
28	80-90	-15.1	-115.9	4.8	1577	0.79	-1.9	2.13	427	72.9	6.3	-45.3	7.05
28	90-100	-15.7	-119.7	5.6	1238	0.62	-1.5	2.15	331	58.0	6.3	-39.2	7.00
28	100-110	-16.0	-122.6	5.5	414	0.20	-1.6	1.00	107	17.7	5.1	-42.2	6.72
28	110-121	-16.1	-123.0	5.5	422	0.20	-2.0	1.36	105	21.0	5.0	-44.6	6.80
28	120-130	-16.4	-126.2	5.1	-	-	-2.3	-	-	-	-	-	-
28	130-140	-16.4	-126.2	5.2	-	-	-3.4	-	-	-	-	-	-
28	140-151	-16.7	-128.0	5.4	-	-	-4.3	-	-	-	-	-	-
29	0-10	-15.5	-119.9	4.4	-	-	-6.7	-	-	-	-	-	-
29	10-20	-15.2	-116.7	5.0	1111	0.55	-6.4	1.56	297	48.2	7.2	-48.7	6.84
29	20-30	-15.1	-115.7	5.5	1198	0.59	-5.7	1.47	324	55.1	5.4	-47.5	6.84
29	30-42	-15.1	-116.3	4.6	1446	0.72	-4.9	1.74	392	67.5	7.0	-50.9	6.99
29	42-50	-15.5	-119.0	4.9	1485	0.74	-4.4	2.05	406	69.9	7.1	-44.8	7.02
29	50-58	-15.5	-118.5	5.3	1427	0.71	-3.9	2.09	383	66.2	6.0	-44.7	7.15
29	60-70	-15.2	-117.0	4.8	-	-	-3.6	-	-	-	-	-	-
29	71-80	-15.5	-119.0	5.1	1455	0.73	-2.6	2.10	388	67.6	6.0	-46.6	7.03

29	80-95	-15.9	-122.2	5.1	621	0.30	-1.5	1.21	163	28.0	4.1	-46.3	6.97
29	95-105	-16.0	-122.7	5.6	509	0.24	-1.1	1.51	128	25.8	3.5	-44.8	6.95
29	105-115	-16.3	-125.5	5.3	-	-	-1.3	-	-	-	-	-	-
29	115-125	-16.5	-126.5	5.4	-	-	-1.1	-	-	-	-	-	-
29	125-135	-16.7	-128.2	5.3	-	-	-0.4	-	-	-	-	-	-
30	0-10	-15.3	-117.4	4.6	-	-	-7.2	-	-	-	-	-	-
30	10-20	-15.2	-117.0	4.9	1581	0.79	-7.1	2.06	431	74.9	6.7		7.66
30	20-30	-15.2	-116.4	5.3	1501	0.75	-6.6	1.88	408	71.1	6.5	-46.4	7.04
30	30-38	-15.2	-116.7	4.8	1637	0.82	-6.3	2.11	447	77.7	8.1	-50.9	7.07
30	42-50	-15.3	-117.5	5.0	1731	0.87	-6.0	2.31	472	82.1	7.8	-46.8	7.31
30	50-60	-15.3	-117.4	5.3	1523	0.76	-5.4	2.04	417	68.4	8.3	-46.4	7.00
30	60-70	-15.5	-118.0	5.6	1648	0.83	-4.6	2.36	444	75.9	8.4	-44.6	6.93
30	70-80	-15.4	-118.4	4.8	-	-	-3.9	-	-	-	-	-	-
30	80-88	-15.5	-119.1	4.7	1400	0.70	-3.6	2.12	375	65.3	6.5	-43.7	7.08
30	88-95	-15.8	-122.0	4.8	445	0.21	-3.3	1.04	114	19.0	6.3	-40.2	6.72
30	95-105	-15.7	-120.3	5.1	600	0.29	-3.2	1.43	154	28.8	6.1	-41.4	6.9
30	105-115	-15.9	-122.1	5.0	839	0.41	-2.7	1.82	218	40.6	7.6	-49.6	7.08
30	114-123	-16.7	-128.1	5.3	-	-	-2.4	-	-	-	-	-	-
30	123-133	-16.5	-126.5	5.6	-	-	-1.3	-	-	-	-	-	-
30	133-143	-16.6	-127.2	5.5	-	-	-0.5	-	-	-	-	-	-
31	0-10	-16.5	-126.6	5.1	-	-	-12.7	-	-	-	-	-	-

31	10-20	-16.6	-127.7	4.7	101.2	0.05	-12.2	1.05	23.4	5.64	85.6	-77.5	7.35
31	20-30	-16.0	-123.2	4.6	645	0.31	-11.3	2.47	161	37.5	193.7	-77.0	7.50
31	30-40	-16.1	-123.8	5.0	1056	0.52	-10.4	3.04	278	53.0	133.1	-57.1	6.96
31	40-50	-15.4	-118.1	4.8	1164	0.58	-9.5	2.72	313	53.0	15.0	-41.3	6.69
31	50-60	-15.2	-116.2	5.2	1273	0.63	-6.7	1.72	351	59.2	10.6	-47.9	6.85
31	60-70	-15.3	-117.3	4.8	1605	0.81	-5.0	1.96	430	71.4	3.0	-45.0	7.28
31	70-80	-15.5	-119.3	5.1	1836	0.93	-5.2	2.53	468	81.4	7.3	-37.5	7.16
31	80-90	-15.8	-121.2	5.5	-	-	-4.4	-	-	-	-	-	-
31	90-100	-15.9	-121.2	6.0	2492	1.28	-3.9	3.25	636	99.8	6.0	-31.8	7.35
31	100-110	-16.1	-122.7	6.4	2708	1.40	-3.4	2.82	695	110	7.0	-40.8	7.69
31	110-120	-16.3	-122.9	7.3	3080	1.60	-2.9	3.36	774	127	4.9	-39.9	7.37
31	120-130	-16.5	-124.8	7.6	3630	1.91	-2.5	3.47	936	149	6.5	-42.4	7.43
31	130-140	-16.6	-126.5	6.6	3610	1.90	-2.1	3.55	924	147	5.6	-39.8	7.37
31	137-147	-16.9	-128.1	6.9	-	-	-1.7	-	-	-	-	-	-
31	147-157	-17.0	-129.0	7.2	-	-	-1.2	-	-	-	-	-	-
31	157-167	-17.1	-129.6	7.2	-	-	-0.7	-	-	-	-	-	-
32	0-10	-16.0	-124.5	3.9	797	0.39	-12.4	1.75	208	37.0	160.7	-79.7	6.64
32	10-20	-16.6	-127.4	5.3	101.5	0.05	-11.9	0.66	24.6	4.56	20.1	-65.8	6.63
32	20-30	-16.0	-123.6	4.8	577	0.28	-11.2	3.31	140	34.7	128.6	-77.8	6.78
32	30-40	-16.0	-122.8	5.2	860	0.42	-10.6	2.33	223	43.8	129.6	-63.0	6.86
32	40-52	-15.1	-115.9	5.0	1144	0.57	-9.8	1.81	302	52.0	34.0	-50.9	6.84

32	52-62	-15.0	-114.3	5.4	1578	0.79	-8.9	2.09	427	72.1	2.9	-42.9	6.90
32	62-72	-15.2	-117.4	4.5	1609	0.81	-7.9	1.99	437	72.4	2.6	-42.1	6.83
32	72-82	-15.5	-118.8	5.5	1767	0.89	-7.1	1.95	484	78.5	3.0	-38.0	6.75
32	82-93	-15.8	-121.0	5.7	2407	1.24	-6.4	2.37	611	98.2	5.7	-39.6	6.81
32	93-104	-16.0	-121.6	6.0	2252	1.15	-6.1	2.28	568	93.3	4.2	-40.3	6.88
32	104-114	-16.3	-124.2	6.3	2663	1.37	-5.9	2.48	671	111	3.5	-43.9	7.00
32	114-122	-16.5	-125.8	6.4	3010	1.56	-5.1	2.74	765	125	2.7	-42.7	7.07
32	122-131	-16.7	-126.7	7.2	3090	1.61	-3.6	2.81	788	128	3.6	-42.6	7.07
32	131-140	-16.9	-126.7	8.7	3210	1.67	-2.2	3.00	853	133	6.8	-48.0	7.02
32	140-148	-17.0	-128.7	7.6	2982	1.55	-1.5	2.71	771	123	10.3	-52.2	7.23
32	148-156	-17.1	-129.1	7.6	2620	1.35	-0.9	2.32	674	106	51.1	-61.9	7.15
32	156-164	-17.1	-129.1	7.5	3520	1.85	-0.6	3.17	908	142	538.7	-69.5	7.24

10 Eidesstattliche Erklärung

Ich versichere, die Masterarbeit selbständig und lediglich unter Benutzung der angegebenen Quellen und Hilfsmittel verfasst zu haben. Alle Stellen, die wörtlich oder sinngemäß aus veröffentlichten oder noch nicht veröffentlichten Quellen entnommen sind, sind als solche kenntlich gemacht. Die Zeichnungen oder Abbildungen in dieser Arbeit sind von mir selbst erstellt worden oder mit einem entsprechenden Quellennachweis versehen.

Ich erkläre weiterhin, dass die vorliegende Arbeit noch nicht im Rahmen eines anderen Prüfungsverfahrens eingereicht wurde.

Potsdam, den _____ _____